This manuscript is a preprint:

This manuscript has been submitted to Tectonics. Subsequent versions of this manuscript may have different content. If accepted, the final version of this manuscript will be available via the 'Peer-reviewed Publication DOI' link via this webpage.

Please feel free to contact any of the authors directly or to comment on the manuscript. We welcome feedback!

Note: Supplementary information that is reference in the text is provided at the bottom of the document.

- 1 Spatial and temporal variations in slip rate over millions of years on an extensional fault system:
- 2 implications for seismic hazard
- 3 Billy. J. Andrews¹, Zoë. K. Mildon¹, Christopher A-L. Jackson^{2,3}, Constanza Rodrigues Piceda¹,
- 4 Francesco lezzi⁴, and Joanna P. Faure Walker⁶
- ¹School of Geography, Earth and Environmental Sciences, University of Plymouth, Drake Circus,
- 6 Plymouth, PL4 8AA, UK
- ⁷ Department of Earth Science & Engineering, Imperial College, Prince Consort Road, London,
- 8 SW7 2BP, UK
- 9 ³WSP UK Ltd, 8 First Street, Manchester, M14 4RP, UK
- ⁴Department of Earth Sciences, Environment and Resources, University of Naples Federico II,
- 11 Naples, Italy
- ⁵School of Natural Sciences, Birkbeck, University of London, Malet Street, London, WC1E 7HX,
- 13 UK

18

- ⁶Department of Risk and Disaster Reduction, University College London, Gower Street, London,
- 15 WC1E 6BT, UK
- 16 Corresponding author: Billy Andrews (billy.andrews@plymouth.ac.uk)

17 **Key Points:**

- Slip rates on normal faults vary by up to 2 orders of magnitude over a few million years
- Within a fault network, the slip rates and the shape of slip rate profiles on individual
 faults are variable during different time periods
- In a network of faults, the recurrence interval for M>5 earthquakes can remain constant over time with the contribution from individual faults varying

Abstract

23

40

- 24 Slip rate is a key input for fault-based seismic hazard assessment, with temporal and spatial
- variations in slip rate along and between faults influencing earthquake size and recurrence.
- 26 Temporal variations in slip rate have been attributed to earthquake clustering and anti-
- 27 clustering in tectonically active settings. Here we explore the combined temporal and spatial
- assessment of slip rate variations of individual faults and the network they form part of. Here
- 29 we present slip rates derived from a seismically imaged, inactive fault network, offshore NW
- 30 Australia. We show spatial and temporal slip rate variations across million-year time scales for
- individual faults within a network of across-strike faults. Slip rate profiles also differed through
- time, with the location of maximum slip rate on individual faults migrating along-strike by
- 33 several kilometres between time periods (over 10⁶ to 10⁷ million years). We then calculate the
- resulting temporal variations in seismic hazard arising from the changes in slip rates. We show
- 35 that within a fault network, whilst overall the earthquake recurrence rates over the entire fault
- system remain similar, recurrence rates on individual faults vary on the million-year timescales
- we study. Spatial and temporal variability of slip rate can introduce uncertainty in earthquake
- probability calculations, highlighting the need to incorporate this into probabilistic seismic
- 39 hazard assessments.

Plain Language Summary

- 41 Understanding how quickly faults move over time, known as their slip rate, is an essential
- 42 element in understanding the seismic hazard posed by an individual fault or fault network. A
- faults slip rate does not remain constant through time, but instead a fault can speed up or slow
- down. Additionally, where faults occur as part of a wider fault network, the proportion of slip
- 45 taken up by a particular fault can vary through time with one fault faster than another at one
- 46 time period, and slower in another. This has a direct effect on the recurrence rates of
- 47 earthquakes, and therefore the hazard posed by individual faults and/or fault networks.
- In this study, we used 3D seismic data to examine an ancient fault network preserved offshore
- 49 NW Austrailia. Although these faults are no longer active, they preserve a record of slip
- spanning millions of years, allowing us to study how slip rates varied across the network over
- 51 these time periods. We found that the speed and location of slip on individual faults changed
- 52 over time, with the areas of maximum slip rate shifting by kilometers along a given fault
- 53 between studied time periods.
- 54 By analysing these changes, we show that whil the total activity of the fault system remained
- 55 broadly consistent across several time periods, individual faults showed large variations in the
- 56 magnitude and shape of their slip rate profiles. It was also found that the whole network sped
- up in the final time period by a factor of 10. These changes directly impact calculated

58	earthquake rates	, and highlights	how the spatial	distribution and	magnitude of	f seismic hazar

59 can vary across a lifetime of an active fault.

1 Introduction

60

- 61 Slip rates are an important input into fault-based probabilistic seismic hazard assessment
- 62 (PSHA) (Chartier et al., 2019; Faure Walker et al., 2019; Pace et al., 2016a; Youngs &
- 63 Coppersmith, 1985), as they influence the moment accumulation rate and, therefore, the
- 64 earthquake occurrence rates (Brune, 1968). Fault-based PSHA relies on the available data
- describing the fault activity, and these are often restricted to one single measurement of slip-
- rate on a fault, that is calculated for a specific period of time (e.g., Gómez-Novell et al., 2020;
- Valentini et al., 2017; Williams et al., 2023) However, slip-rates on both active and inactive
- 68 faults are known to vary over decadal to million year timescales (Friedrich et al., 2003; G. P.
- 69 Roberts et al., 2024). Most previous studies into temporal slip-rate variability have focused on a
- single along-strike location on a fault, for example paleoseismic trenching studies (e.g. (Dolan et
- al., 2016; A. Nicol et al., 2010; Onderdonk et al., 2015; Wechsler et al., 2018; Zinke et al., 2019)
- or cosmogenic isotope studies (Goodall et al., 2021; Mechernich et al., 2018), although some
- studies do integrate numerous single locations across a region to discuss the broader behaviour
- of the fault network (Cowie et al., 2017; Dolan et al., 2007a; lezzi et al., 2021; Mildon et al.,
- 75 2022; A. Nicol et al., 2010; G. P. Roberts et al., 2024; Sgambato et al., 2025). For normal faults,
- maximum displacement (and thus slip rate) is commonly observed near the centre of the fault,
- and displacement (or throw) profile are commonly assumed to show a broadly bell-shaped,
- elliptical or triangular form (Cowie & Scholz, 1992; Manighetti et al., 2004; Manzocchi et al.,
- 79 2006; Nicol et al., 2005; Roberts, 2007). However, slip rates and total displacement show
- further variability along-strike (J. A. Cartwright & Mansfield, 1998; Faure Walker et al., 2009,
- 2010, 2012, 2019; lezzi et al., 2020; McClymont et al., 2009; Gerald P Roberts & Michetti, 2004;
- 82 Sgambato et al., 2020).
- 83 The effect of spatial-temporal variations in slip-rate of the kind described above on PSHA
- remains relatively understudied (Faure Walker et al., 2019; Pace et al., 2014; Roberts et al.,
- 85 2024; Scotti et al., 2021). Faure Walker et al. (2019) investigated how along-strike changes in
- 86 slip-rate on a single fault affect the resulting seismic hazard. They found that different shapes of
- 87 slip-rate profiles affect the resulting seismic hazard curves, with probability calculations varying
- 88 for different profiles shapes beyond the uncertainty of Ground Motion Prediction Equations.
- 89 This highlights the importance of collecting high-spatial resolution slip rate data. However, as
- 90 slip-rate can also vary temporally, the magnitude and the position of maximum slip along an
- individual fault may also vary through time (Benedetti et al., 2002, 2013; Cowie et al., 2017;
- 92 lezzi et al., 2021; Roberts et al., 2024, 2025), and thus the location of maximum slip within a
- 93 fault network may also vary. Understanding how throw accumulates through time, and
- 94 therefore how slip-rate evolves, is an important consideration for seismic hazard assessments
- 95 (Figure 1a). By investigating how much natural variability in slip-rate evolution might be

expected, this can be incorporated as a source of uncertainty in fault-based PSHA (e.g. Cowie et 96 97 al., 2017; Roberts et al., 2025). 98 Faults do not occur in isolation but instead form networks of relatively closely spaced 99 structures. It is well-established that faults within broader networks interact over a range of temporal (decadal to million years) and spatial (10s m to >100 km) scales, directly controlling 100 101 their slip rate and the related earthquake parameters (e.g., recurrence and magnitude). The mechanisms of fault interaction can include co- and interseismic stress changes (Gupta & 102 103 Scholz, 2000; Harris & Simpson, 1998; Stein, 1999), the stress interaction between lower-crustal shear zones to which upper-crustal faults are geometrically and kinematically connected 104 105 (Mildon et al., 2022; Roberts et al., 2024), and strain localisation (Cowie et al., 2005; A. Nicol et al., 1997; Nixon et al., 2024). Short-timescale fault interaction has in places been considered 106 107 within seismic hazard studies, either via Coulomb stress changes (Pace et al., 2014; Toda &

Enescu, 2011; Toda & Stein, 2018; Verdecchia et al., 2019) or by testing different fault

segmentation scenarios and their potential to produce multiple fault ruptures (Mignan et al.,

2015; Milner et al., 2013). Over longer time scales (i.e., > Myrs), while it is well-established that

faults interact, affecting their throw accumulation (e.g., Childs et al., 2019; Fossen & Rotevatn,

2016; Nixon et al., 2024; Pan et al., 2022), it is unclear how fault interactions will affect

calculated earthquake rates across the network, contributing to the regional seismic hazard,

114 compared to earthquake rates on individual faults, which mainly affect local seismic hazard) 115 (Figure 1b).

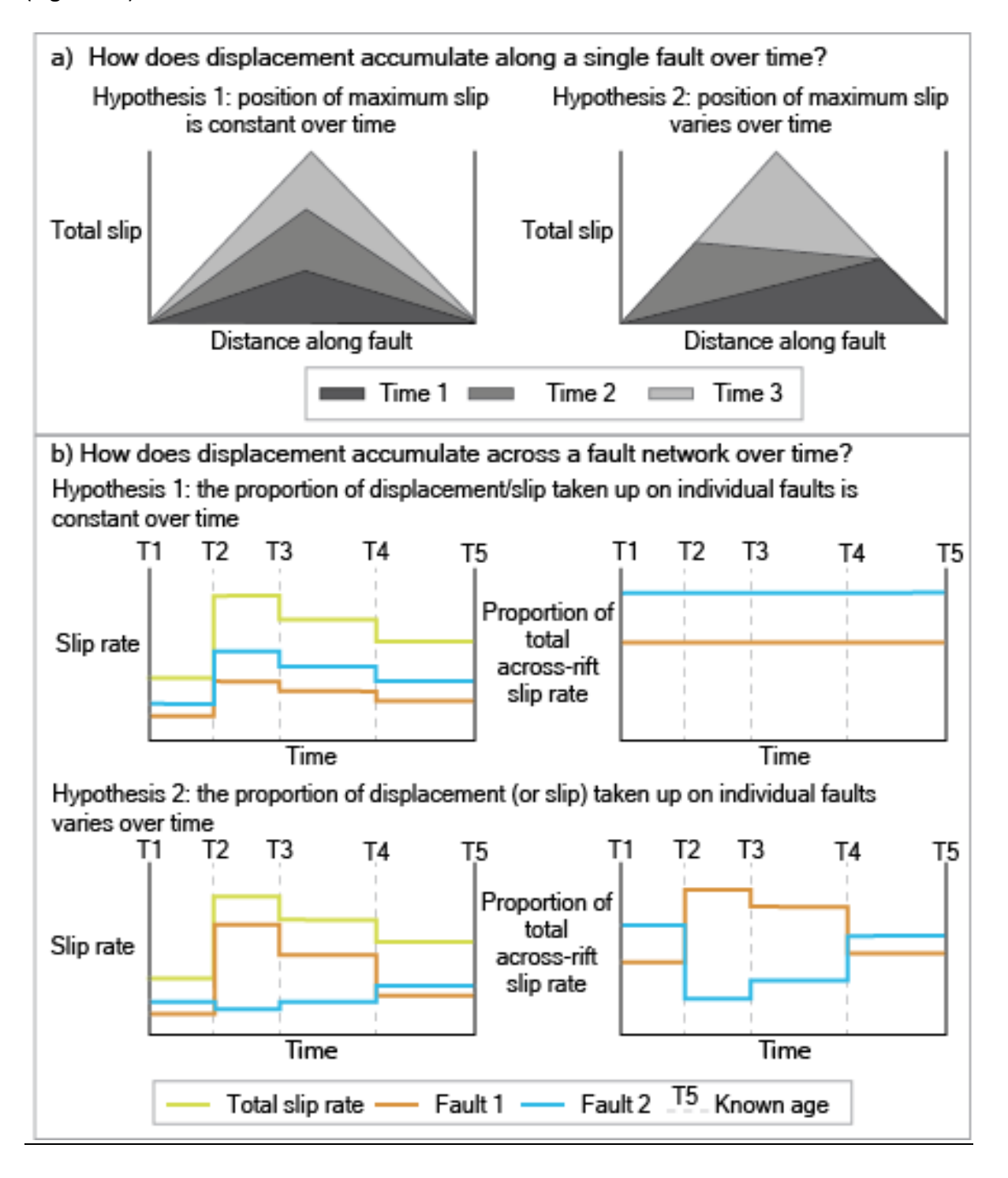


Figure 1 – Two questions and associated hypotheses that will be tested in this study.

117

3D seismic reflection surveys can be used to investigate slip rate variability over long timescales (>Ma). Stratigraphic successions imaged and used to infer slip-rate patterns are often deposited over tens of millions of years, far longer than timescales typically resolved for presently active faults, enabling long-term variations in slip rate to be explored. Several assumptions and limitations must be considered when using 3D seismic data including subjective bias of the interpreter (Andrews et al., 2024; Bond, 2015), the need for sedimentation rates to exceed throw rates (Jackson et al., 2017), uncertainties and resolution of age data relating to mapped reflectors (e.g., Reeve et al., 2016), and the need of a reliable velocity model to convert throw and fault dip from time to meters (Holden et al., 2024) which can also introduce uncertainties in the interpreted fault dip. Despite these caveats, 3D seismic reflection dataset image the full three-dimensional geometry of faults, allowing us to explore spatial patterns in slip-rate with a dense sample spacing (100 m), and at multiple structural levels. Additionally, slip-rate profiles can be used to infer how fault length, and therefore the maximum expected earthquake magnitude, evolved through time. Such measurements are often not possible on active faults, where the along-strike exposure of the fault is limited to the present-day surface, may not be continuous, and/or the geomorphology may not be appropriate to extract slip-rate values.

In this study, we address two key questions related to the slip rate variability in a normal fault network. The first question is: how does displacement accumulate along a fault over time? We test two hypotheses: (1) the position of maximum slip remains fixed over time, or (2) it varies temporally. To address these hypotheses, we construct fault slip histories across a kinematically linked normal fault network over four to eight time periods spanning 72.2 million years. This analysis is based on a 3D seismic reflection survey from offshore NW Australia, a region that experienced Jurassic and Cretaceous rifting, which resulted in the formation of an extensive normal fault network. We interpret several age-constrained seismic horizons, dated using wells within the study area, and use horizon offsets and ages to infer slip rates along selected faults. We first document the spatial and temporal variability of slip rates along a single, geometrically isolated fault, before expanding to consider the broader fault network. The second question we address is how does displacement accumulate across a fault network over time? (Figure 1b). We test two hypotheses: (1) the proportion of displacement taken up by individual faults is constant over time, or (2) the proportion of displacement taken up by individual faults varies. Finally, we use the derived slip rates to infer how the average annual earthquake occurrence rate would have changed through time and discuss the implications of our findings for seismic hazard assessment.

2 Geological setting

118119

120

121122

123

124125

126127

128

129

130131

132

133

134135

136

137

138

139140

141

142

143

144145

146147

148

149

150

151

152

153

This study focuses on a fault network situated in the Exmouth Plateau region of the Northern Carnarvon Basin, offshore NW Australia (Fig 2a, b). The ~400 km wide Exmouth

154	Plateau lies outboard of several sub-basins (Fig 2a) and is characterised by a complex
155	tectonostratigraphic history (Bilal & McClay, 2022; Gartrell et al., 2016; Gartrell, 2000). The
156	area experienced three main phases of extension: 1) NW-SE directed extension during the Late
157	Carboniferous to Permian that imparted a structural grain across much of the Northern
158	Carnarvon Basin (Bilal & McClay, 2022; Deng & McClay, 2019, 2021; Etheridge & O'Brien, 1994;
159	Gartrell, 2000), 2) Lower to Middle Triassic extension evident across west-dipping NE-SW to
160	NNW-SSW normal faults (Bilal & McClay, 2022), and 3) Upper Triassic to Middle Jurassic (209.5
161	to 162.5 Ma) ~E-W directed extension that caused wedge-shaped growth strata to develop
162	along N-S to NNE-SSW trending faults (Bilal et al., 2020; Bilal & McClay, 2022; Black et al., 2017
163	Karner & Driscoll, 1999; Lathrop et al., 2021) (Fig. 2c) – this is the phase of extension that we
164	focus on. Between the Lower to Middle Triassic extension, and initiation of Upper Triassic
165	extension, a ~400 m thick succession of fluvio-deltaic sandstones and mudstones of the
166	Mungaroo formation blanketed the earlier phase of extension. Following the main phases of
167	extension (162.5 to 137.3 Ma), minor throw accumulation continued with local fault
168	reactivation, tip propagation, and abundant sills, dykes and dyke-induced faults during an
169	otherwise post-rift phase (Black et al., 2017; Direen et al., 2008; Magee et al., 2023; Magee &
170	Jackson, 2020a, 2020b). This was followed by the deposition of passive margin sequences

(137.3 to 0 Ma) following continental breakup during a period of thermal subsidence and passive margin development (Black et al., 2017; Direen et al., 2008).

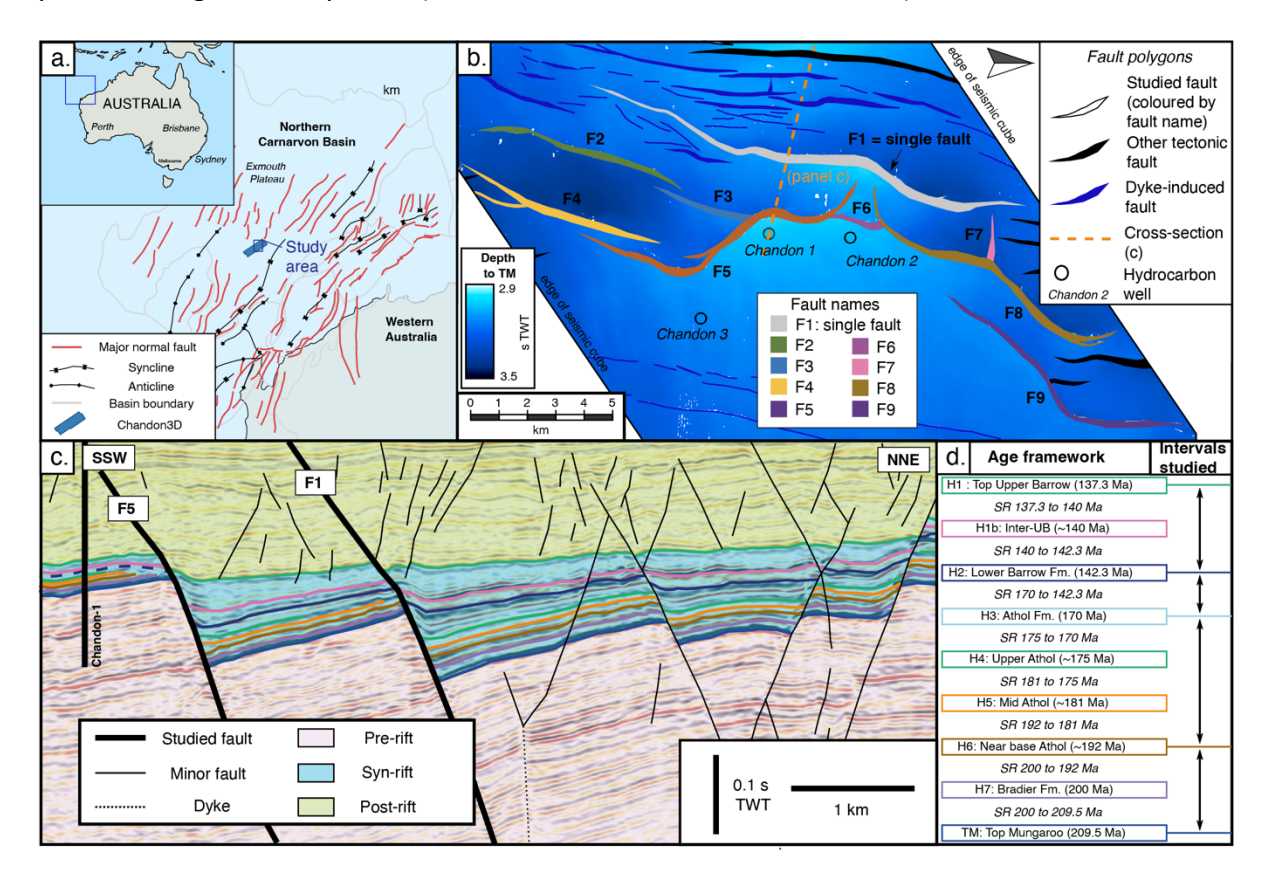


Figure 2 – Overview of the Chandon 3D seismic cube used in this study. a) Location of the Chandon 3D seismic cube. b) Depth to base syn-rift horizon (Top Mungaroo, TM) showing the locations of faults and the distribution of throw across the area. Open circles show the locations of wells used to provide age constraints on the stratigraphy of the area. The single fault with relatively simple geometry that is first studied is indicated. The studied fault network is shown as black fault polygons. c) Seismic cross-section across the fault network of interest, showing the key horizons and ages used in this study. d) Stratigraphic age framework used to determine the slip rates over different time periods, where the ages are given with a ~, these are approximate ages based on constant sedimentation rates, and where ~ is not present, the ages refer to local ages derived from well reports (see main text for further discussion on age related uncertainties).

In this study, we explore slip-rate evolution from the Upper Triassic (209.5 Ma) through to the end of the post-rift phase (137.3 Ma). The Exmouth Plateau was starved of sediment input throughout active rifting (Reeve et al., 2016, 2022). This caused large offset faults to have a surface expression at the time of faulting and undergo footwall degradation, and most faults to have condensed footwall stratigraphic successions (Bilal & McClay, 2022; Karner & Driscoll,

1999). The faults in our study area show no evidence of footwall degradation and most horizons are preserved on both the footwall and hanging wall of all faults, suggesting subsidence rate exceeded sediment accumulation rate for the studied fault network. Following the main phase of extension, some major faults in the Exmouth Plateau underwent 'tip-retreat', whereby fault length decreases with continued throw accumulation (Lathrop et al., 2022). The long-lived nature of the studied faults and lack of footwall degradation enable us to explore how slip rate differs through space and time across a complex fault network over >70 Myr.

3 Methods

- 3.1 Seismic reflection interpretation and data extraction
- 3.1.1 Seismic reflection data

The fault network in this study is imaged in the Chandon3D seismic cube (Fig 2), a 3D, time-migrated, zero-phase seismic reflection survey that has a record length of 6 s two-way-time (TWT) and a bin spacing of 25 m. Seismic data is displayed in SEG reverse polarity, where a downward increase in acoustic impedance corresponds to a trough (black) reflection, and a downward decrease in acoustic impedance corresponds to a peak (red) reflection. The spatial resolution within the interval of interest (2.9 to 3.4 s TWT) is estimated by calculating the limits of separability (the minimum vertical distance whereby interfaces will produce distinct reflectors, ~17-21 m) and visibility (the vertical distance where interfaces are indistinguishable from background noise, 2-3 m) (Brown, 2011).

3.1.2 Borehole data and age framework

To constrain the age and lithology of mapped reflectors, we tied four different boreholes (Chandon-1, Chandon-2, Chandon-3 and Yellowglen, located 25.5 km west of Chandon-1) to the survey, with well reports available through the Geoscience Australia Portal (https://portal.ga.gov.au/). Boreholes were drilled into the footwalls of tilted blocks and extend into the upper portion of the Mungaroo Formation. They contain information about the depth and age of formation tops, alongside geophysical information such as gamma ray, sonic, neutron porosity, and bulk density data. We use age data derived from biostratigraphic information reported in the well reports to constrain the age of five reflectors between the Top Mungaroo (209.5 Ma) and the Top Upper Barrow (137.3 Ma) Formations. Due to stratigraphic thinning of the footwall, some regional reflectors are not observed in the boreholes (e.g., subdivisions of the Athol Formation). To account for this, and to expand our age framework we

- inferred the age of an additional four reflectors assuming constant sedimentation rates
- between age constrained reflectors (after Lathrop et al., 2021; Pan et al., 2022).
 - 3.1.3 Seismic interpretation and calculation of slip rate

223

224

225

226

227

228229

230231

232

233234

235

236

237

- Slip rate can be calculated for faults where subsidence rate exceeds throw rate and the age of mapped horizons are known (e.g., due to well ties) (e.g., Lathrop et al., 2021; Nicol et al., 2005; Pan et al., 2022; Childs et al., 2003). In this study we interpret nine age constrained reflectors that could be mapped across the studied fault network to investigate slip-rate variations across eight time periods (Fig 2d). To extract throw across each mapped horizon, we construct fault-perpendicular transects (e.g. Fig. 2c). Sampling was undertaken by transposing this line by 100 m, with the orientation of the transect adjusted where fault strike changed by > 15° to mitigate against obliquity errors (Andrews et al., 2024). At each sample location, we collect fault cut-off data that includes near-fault continuous deformation for each horizon by projecting the regional dip of the horizon onto the fault plane and measuring the projected footwall and hanging wall horizon-fault plane cut-off pairs (Figure S1). Continuous deformation will account for the long-term strain accumulated on the fault and includes non-discrete strain (e.g., folding) and/or brittle deformation that is below the limit of separability of the dataset
- Cut-off pairs are converted from TWT to meters by using a velocity model constructed by fitting a polynomial best fit to the combined check-shot data from the nearby wells (Supplementary 1) and used to calculate throw for each horizon. To calculate slip-rate across two horizons (H1 and H2), the difference in throw is calculated as:
- 242 $\Delta throw = throw_{H2} throw_{H1}$ (Equation 1)

(e.g., Childs et al., 2017; Delogkos et al., 2020).

- For cases where Δthrow is positive, indicating accumulated slip across the horizons, we used the dip across H2 to convert Δthrow to the change in slip:
- $slip(m) = \frac{\Delta throw}{\sin(dip_{H2})}$ (Equation 2)
- Equation 2 assumes that displacement across the fault is purely dip-slip (i.e., the slip vector is perpendicular to the measurement transect), and that the present-day dip of the fault can be considered representative of fault dip at the time of extension. If Δ throw is <0, indicating no slip accumulation, slip-rate will be zero at this location. We then used Δ slip to calculate the slip-rate
- by dividing by the difference in age between H1 and H2 (Equation 3):

251 Slip rate
$$\left(\frac{mm}{yr}\right) = \frac{\Delta Slip_{H2H1} \cdot 1000}{Age_{H2} - Age_{H1}}$$
 (Equation 3)

We repeated these calculations at each paired cut-off, as well as for the deepest and shallowest mapped horizons, to calculate the rift-averaged slip rate. For the latter, we used a rift-average dip (dip_{RA}) to convert Δ throw to Δ slip by considering the difference in depth and horizontal distance between the footwall pick across H1 and the hanging wall pick across TM.

3.1.4 Uncertainty in our slip rate calculations

252253

254

255

256

257

258

259260

261262

263264

265

266

267

268

269

270

271272

273

274275

276

277

278

279280

281282

283

284

285

286

In this section we describe the uncertainties associated with the calculation of slip rate and the methods used to address them:

Age of mapped horizons: Uncertainty in horizon age may arise from errors in formation ties or from uncertainties and/or the vertical spacing of biostratigraphic data used to derive formation ages from well data. This is the case for the Mesozoic succession, where published ages differ across the Exmouth Plateau. For instance, the Top Mungaroo (TM) has an age of 209.5 Ma within the sample area, whereas elsewhere in the Exmouth Plateau it ranges from 210 to 204 Ma (Reeve et al., 2022). In this study, we take ages from local well reports as we are interested in relative changes in slip-rate across a fault network and not across the basin. Additional uncertainty in age occurs where we have inferred age based on constant sedimentation rates. If this assumption does not hold, then the absolute slip-rate between time periods bounded by these reflectors may be either overestimated or underestimated relative to the true value. However, as the same age is used throughout the study area, these horizons with inferred ages act as 'time-lines', and the shape of slip-rate profiles as well as relative sliprate between faults within that time period will be unaffected by this uncertainty providing a greater temporal resolution of slip rate variations across the network. To account for uncertainty in absolute horizon age, we apply a 0.25 Myr error to horizon ages when calculating minimum and maximum slip-rate values. We consider this to be sufficient to account for uncertainties within the study area whilst also considering local ages derived from wells to be reliable.

Horizon mapping and correlation across faults: Horizon picks rely on consistent waveform reflections (Brown, 2011), and as this study requires information about the age of the reflector, horizons should ideally be linked to well data (Schaaf & Bond, 2019). To mitigate uncertainties and ensure consistency across the study area, we selected a fault network near three wells (Fig 2b), allowing horizons to be mapped confidently around fault tips (Bond, 2015; Chellingsworth et al., 2015). Whilst the significant footwall degradation observed elsewhere in the Exmouth Plateau (Barrett et al., 2021; Bilal et al., 2020; Martinez et al., 2024) was not present in the study area, footwall stratigraphy was sometimes condensed, locally hindering the mapping of horizons. Where a horizon is only missing in the footwall, we take the cut-off of the next youngest horizon as the footwall cutoff, thereby constraining the minimum throw

across this specific horizon. Where the horizon is missing on both sides of the fault, slip rate is calculated for this sample point using the Δ throw to the next youngest horizon (i.e., if H2 was missing, slip rate would be calculated between H3 and H1).

Fault interpretation: Uncertainties in fault interpretation stem from an interpreter's conceptual model of the study area, seismic reflection strength, image quality and vertical exaggeration (Alcalde et al., 2017; Schaaf & Bond, 2019). To limit any differences across the study area, we maintained a constant vertical exaggeration (~1:3), and as the reflectors are well-imaged in the interval of interest and our interpretations conform to the region's tectonics (Fig 2c), anticipate minimal and consistent uncertainty in interpreting the position of faults.

Cut-off extraction: The interpretation of how reflections intersect faults (i.e., cut-offs) involves uncertainty influenced by the type of measured cut-off (discontinuous or continuous), the obliquity of the measurement transects, and the positioning of the horizon and fault (Andrews et al., 2024; Faleide et al., 2021; Magee et al., 2023). These uncertainties affect the extraction of key fault parameters used in our slip-rate calculations (e.g., throw, dip). To mitigate against obliquity errors, all cut-off pairs are picked on a transect with a measurement obliquity of <15°. Throw values that take into account continuous deformation introduce more uncertainty that those that do not due to the interpreter having to extrapolate regional dip onto the fault plane (Andrews et al., 2024). However, because the initial stage of fault growth across the Exmouth Plateau includes localised monocline development (Pan et al., 2022), continuous deformation needs to be considered in in our investigation of long-term slip-rate. To account for uncertainties in throw and dip, we applied error values of the greater value of ±8% or ±3 m for throw and ±14% or ±5° for dip, consistent with values reported by Andrews et al. (2024) from the same seismic cube.

Depth conversion: The method used for depth-conversion can influence the extracted fault parameters (Holden et al., 2024). In our study, we employed a polynomial fit to check-shot data. Given that the depth of the studied faults is similar and throw across faults modest (<456 m), any errors arising from the depth conversion are internally consistent in the study and are thus not considered with the throw errors used to calculate slip-rate.

Compaction-related loss of throw: The studied faults are deeply buried (i.e., 2 to 3 km), meaning compaction could rotate faults to less than their syn-extensional dip (Allen & Allen, 2013), thereby reducing throw across syn-sedimentary faults by <15% (Taylor et al., 2008). In this study, we do not undertake decompaction due to the similar depth of the faults, relatively uniform lithologies (Bilal & McClay, 2022), and uncertainties in decompaction parameters, particularly for the hanging wall sediments that are not penetrated by wells. Consequently, our slip-rate estimates represent a minimum, noting post-slip compaction, whilst affecting absolute

values, is thought to have a negligible effect on the overall patterns of slip-rate across the fault network (Taylor et al., 2008).

To account for uncertainties in slip rate (SR) estimates, we calculate the minimum (SR_{min}) and maximum (SR_{max}) values for each paired horizon by using the propagating individual errors applied to our throw, dip, and age data through equations 1-3. Despite the uncertainties, the seismic reflection dataset allows us to explore the spatial-temporal evolution of slip rate at 100 m intervals along each fault, providing useful insights into the long-term evolution of faults and fault networks.

3.1 Seismic hazard modelling

322323

324

325

326327

328

329

330

331332

333334

335

336

337

338

339

340341

342

343

344

345

346

347

348349

350

351352

353

354

To investigate the effect of variable slip rate and changes in fault length observed across the studied fault network we use the MATLAB package FiSH (Pace et al., 2016a), to calculate the expected earthquake occurrence rates across four time periods (209.5 to 192 Ma, 192 to 170 Ma, 170 to 142.3 Ma, and 142.3 to 137.3 Ma) for two examples: 1) a single fault with a relatively simple geometry (i.e., limited sinuosity and no hard linkage to nearby faults); and 2) a fault network that includes the single fault (see Table S4.1 for input parameters). FiSH derives expected earthquake rates based on fault data such as fault length, slip-rate, fault dip, seismogenic thickness, and established empirical relationships (Pace et al., 2016a). For fault dip and slip-rate we take the arithmetic mean of all picks along a given fault, using rift average dip to limit horizon specific errors. The along-fault length (i.e. considering the presence of fault bends, not tip-to-tip length) is extracted based on slip-rate profiles. FiSH requires the seismogenic thickness (aka depth extent of the fault) to be input to calculate the area of the fault surface. We take a slightly different approach herein because (a) faults may extend below the surveyable depth and (b) we cannot constrain the seismogenic thickness when these faults were active. Instead, to calculate the depth extent of the faults, we assume faults have a constant length to height aspect ratio of 2.15 (A. Nicol et al., 1996), although we note that a wide range of fault aspect ratio values exist (Roche et al., 2013; Soliva et al., 2006; Torabi & Berg, 2011). This approach was adopted instead of using a consistent fault width (e.g., extending to the seismogenic thickness of the crust), which would lead to unrealistic fault surface geometries, particularly for short faults. If these assumptions are incorrect, and the faults have larger or smaller aspect ratios, then the resultant earthquake magnitudes would be higher or lower respectively. Although the studied faults are not presently active, our aim is to constrain how earthquake rates change as the slip rates within a fault network changes over different time periods and to investigate how seismic hazard could vary.

4 Results

355

356

357358

359360

361362

363

4.1 Single fault (Fault 1)

To first investigate how slip rates vary along a single fault through time, we choose a single fault (Fault 1) that is physically (if not mechanically and kinematically) isolated from other nearby faults and is relatively geometrically simple (i.e. limited changes in strike and dip). We extract total displacement over the total lifetime of the rift (Figure 3a), as well as displacement over four different time periods (Figure 3b-e). For the four time periods, the displacement is converted to slip rate using the ages of the offset horizons (see Figure 2d for the age framework).

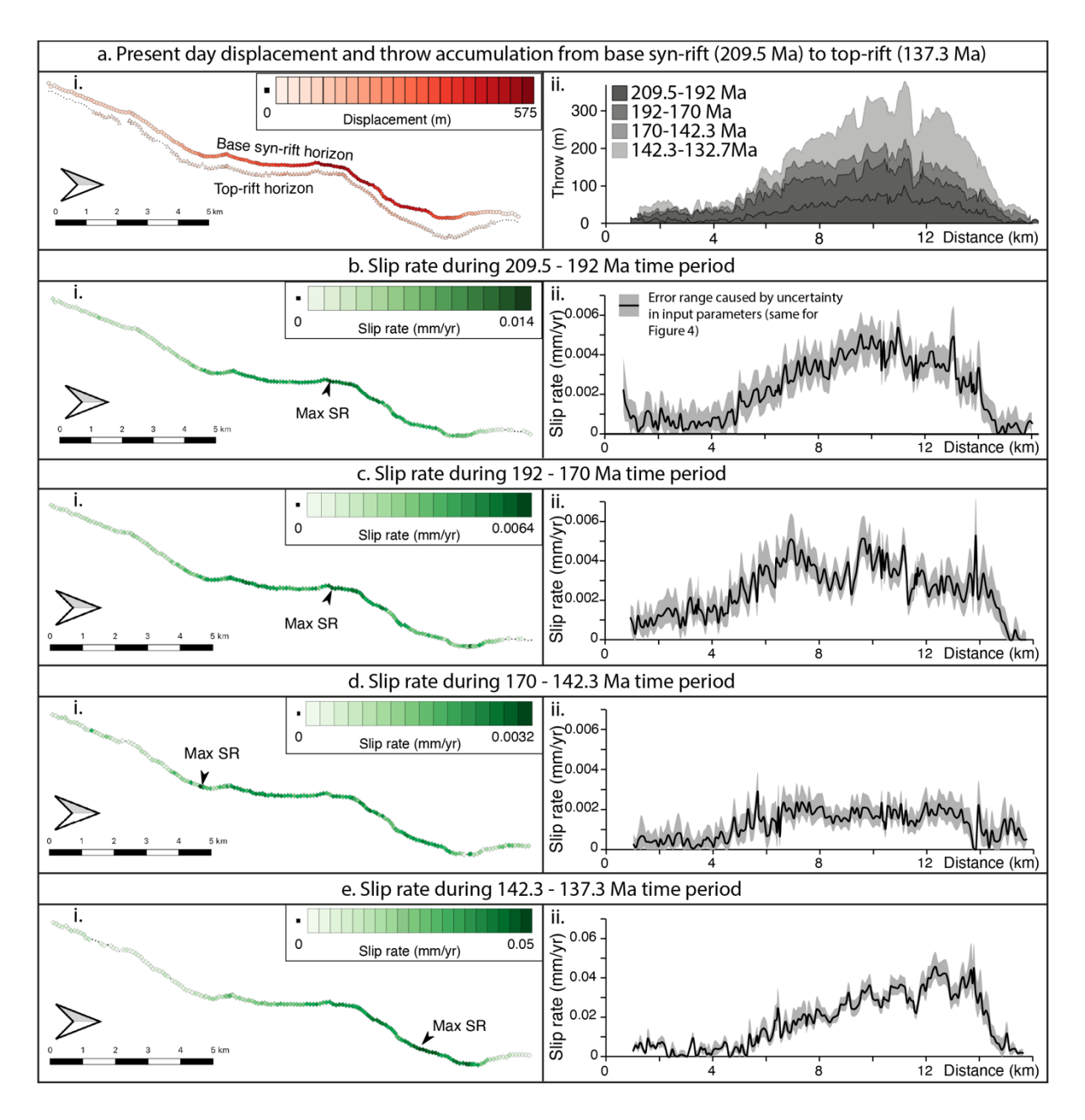


Figure 3 – Variation of slip rate through time along a single fault with relatively simple geometry. a. i. Present day geometry and throw at the base syn-rift (TM, Top Mungaroo) and the top rift horizon (H1, Top Upper Barrow). ii. The cumulative throw plotted for the four studied time intervals between 209.5 and 137.3 Ma and plotted against distance along the fault trace. b-e. Slip rates during different time periods, plotted as i) a colour scale along the fault trace in map view and ii) against distance along the fault (with errors shown by grey dashed lines). Note that the colour scale and vertical axis change scale in each of these sub-plots. Both the magnitude of slip rate and the shape of the slip rate profile changes throughout time.

Considering the total displacement (Figure 3ai), the displacement profile has higher displacement in the centre of the fault, with a slight skew to the northern end of the fault, and lower displacement at the fault tips.

The slip rate in four different time periods is calculated and plotted in map-view (Figure 3b-e, i) and as distance along the fault (Figure 3b-e, ii). Slip is recorded along the full length of the fault for all time periods, suggesting the fault established its length within the first time period (i.e., following a constant-length model of fault growth (e.g., Rotevatn et al., 2019). Across the different time periods, the magnitude of slip rate is variable over the rifting period. Between the first (209.5-192 Ma, Figure 3b) and second periods (192-170 Ma, Figure 3c), the slip rate on the fault decreases, with the maximum slip rate remaining constant $0.0054^{+0.001}_{-0.0008}$ mm/yr to $0.0053^{+0.0018}_{-0.0001}$ mm/yr, although the mean slip rate slightly increases from $0.0023^{+0.0009}_{-0.0007}$ mm/yr to $0.0026^{+0.0008}_{-0.0007}$ mm/yr. The second and third time periods (170-142.3 Ma, Figure 3c) are also characterised by a decrease in slip rate, with the maximum slip rate reducing from $0.0053^{+0.0018}_{-0.0011}$ mm/yr to $0.0029^{+0.0009}_{-0.0007}$ mm/yr, and the mean slip rate approximately halving from $0.0026^{+0.0008}_{-0.0007}$ mm/yr to $0.0013^{+0.0006}_{-0.0005}$ mm/yr. The final period (142.3-137.3 Ma, Figure 3e) contrasts with earlier ones, in that the slip rate increases by an order of magnitude, with the maximum slip rate increasing from $0.0029^{+0.0009}_{-0.0007}$ mm/yr to $0.016^{+0.0018}_{-0.0006}$ mm/yr, and the mean slip rate from $0.0013^{+0.0006}_{-0.0005}$ mm/yr to $0.016^{+0.0004}_{-0.006}$ mm/yr.

In addition to variability in the magnitude of maximum and mean slip rate, the shape of the along-strike slip rate profile also varies with time (Fig 3). The position of maximum slip rate measured along the fault changes over time (indicated on Figure 3b-e, i), but these may be localised maxima relating to a single point on the fault (e.g. Figure 3di). However, variations are also observed in the overall shape of the slip-rate profile (Figure 3b-e, ii). For example, the slip rate profiles are less skewed towards the northern end of the fault in the first two periods (Fig. 2b-c,ii), whereas in the third period, the profile is more elliptical than triangular (Fig. 2dii). In the final period, the shape of the profile (Fig. 2eii) is similar to the long-term profile (i.e. the whole rifting phase, Figure 3aii); this is likely because the higher slip rate (~10x times greater than other time periods) in the final time period has a large impact on the long-term profile.

4.2 Fault network

The fault above occurs within a fault network comprising nine faults, some of which are physically linked (Figure 4a). One fault, Fault 7 is perpendicular to the other nine faults and we therefore omit it from our analysis of along-strike trends across the fault network (Figure 4a).

Considering the total displacement across the network, many of the faults show higher throw near their centres across all time periods (e.g., Faults 1, 4 and 8; Figure 4ai). Note that

due to the ~2.5 km section of Fault 4 that shows no slip during the earliest time period (Figure 4b), this fault is characterised by multiple strands during this period (Figure 4b), but that over time the tips of these strands grew and coalesced to form a single structure by 192 Ma (Figure 4c). The cumulative throw across each individual fault over the four periods studied is plotted in Figure 4aii, as well as the total along-strike throw profile (which sums the throws perpendicular to the orientation of the network).

Along-strike profiles of slip rate for each fault are plotted for each period, with the profiles for individual faults aligned for easy across-strike comparison. While complex, there are several key observations. First is that, like for the single fault, the magnitude of slip rate of individual faults and the entire fault network varies over time, and that all faults increase their slip rate in the final period (142.3-137.3 Ma, note the different vertical scale in Figure 4e). Second, the shape of the along-strike slip rate profile varies for individual faults over time; for example, Fault 2 has a profile that is relatively flat in the first two periods (209.5-192 Ma and 192-170 Ma, Figure 4b and c), near-triangular in the third period (170-142.3 Ma, Figure 4d), and skewed towards its northern end in the final period (142.3-137.3 Ma, Figure 4e). In addition to the variable slip rate profile on individual faults, the shape of the cumulative or summed profile

- varies over time; for example, in the third period, slip is skewed towards the southern end of
- the fault network (Figure 4d).

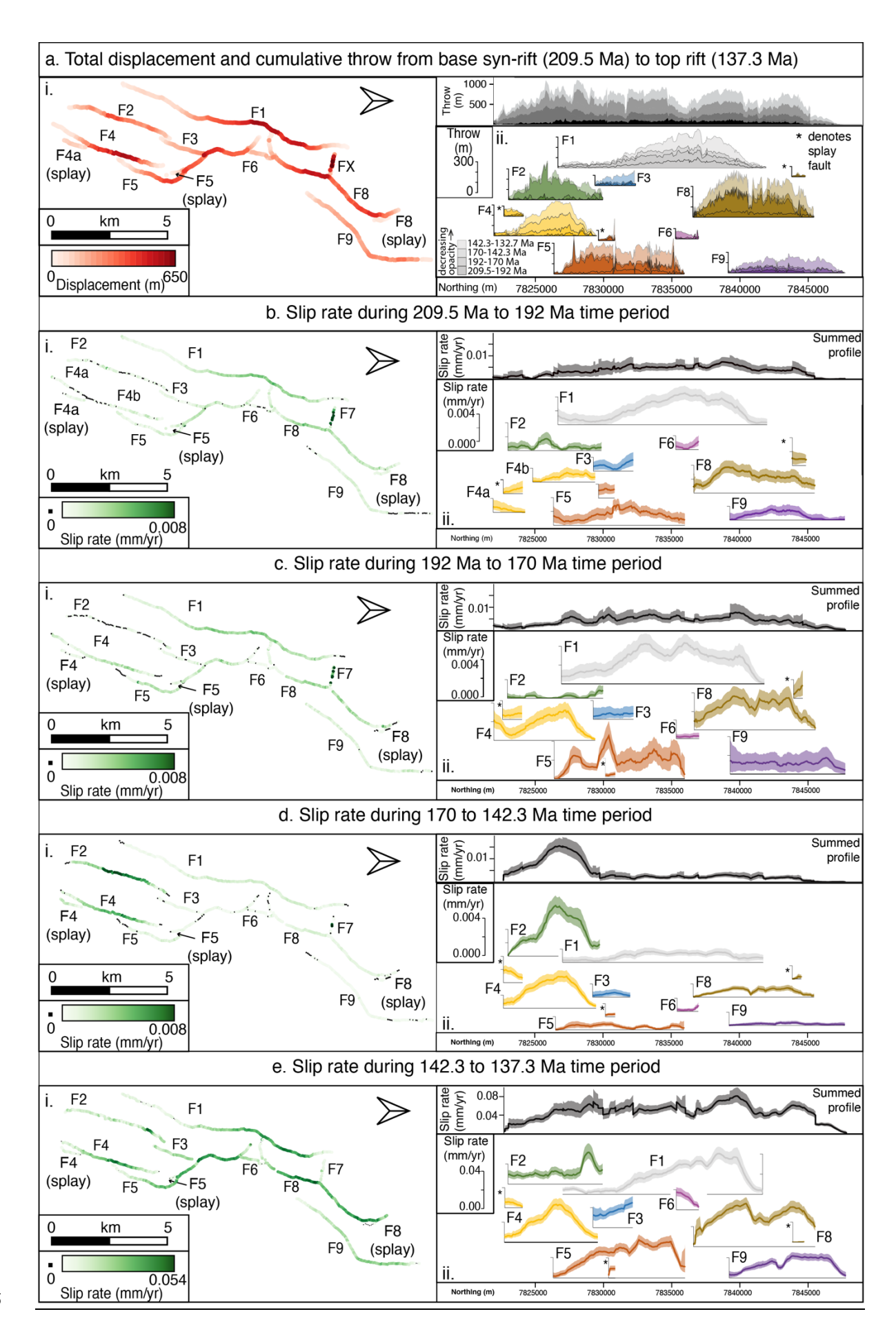


Figure 4 – Along-strike variations in slip rate across the fault network. a) Present day throw across the i) base syn rift horizon (TM) and ii) cumulative throw plots for individual faults and the fault network. Each shade in the cumulative throw plots represents the throw accumulated in a specific time period, the solid colour represents the throw accumulated in the earliest time period, the lighter colours are for later time periods, and the colours match those used in Figure 5. b-e) Slip-rate shown in both map view and as profiles for the four studied time periods. To enable overall profile trends to be explored, the data was smoothed using a window sample of 10 datapoints, for raw data please see Supplementary 3. Note that Fault 4 is two separate faults (4a and 4b) in the first time period (b), and they coalesce together in later time periods. Also, the colour scales of panels i and vertical scales in panels ii differ to better show the trends within a given time period.

We select six transects through the fault network, orientated approximately perpendicular to its overall trend, to study how the slip rate varies over time and throughout the fault network. For the transects, we can investigate variations in slip rate with a higher temporal resolution, resolving all eight time periods shown in Figure 2d. The location of transects was chosen such that temporal variation in slip rate can be explored at key alongstrike locations, capturing different faults and encompassing a different number of across-strike faults (Figure 5a). In all transects, the rapid acceleration of slip rate towards the end of rifting can be seen in Figure 5bi, consistent with the observations from the single fault.

For each transect (Figure 5c-h), the slip rate on each individual fault is measured and plotted over time (Figure 5c-h, i). To enable comparison and to investigate how the dominance of different faults changes over time, we calculate and plot the percentage of total slip rate accommodated on each fault across the transect (Figure 5c-h, ii). This indicates how the

- extension is being shared across the fault network, and whether this remains constant or varies
- 450 over time.

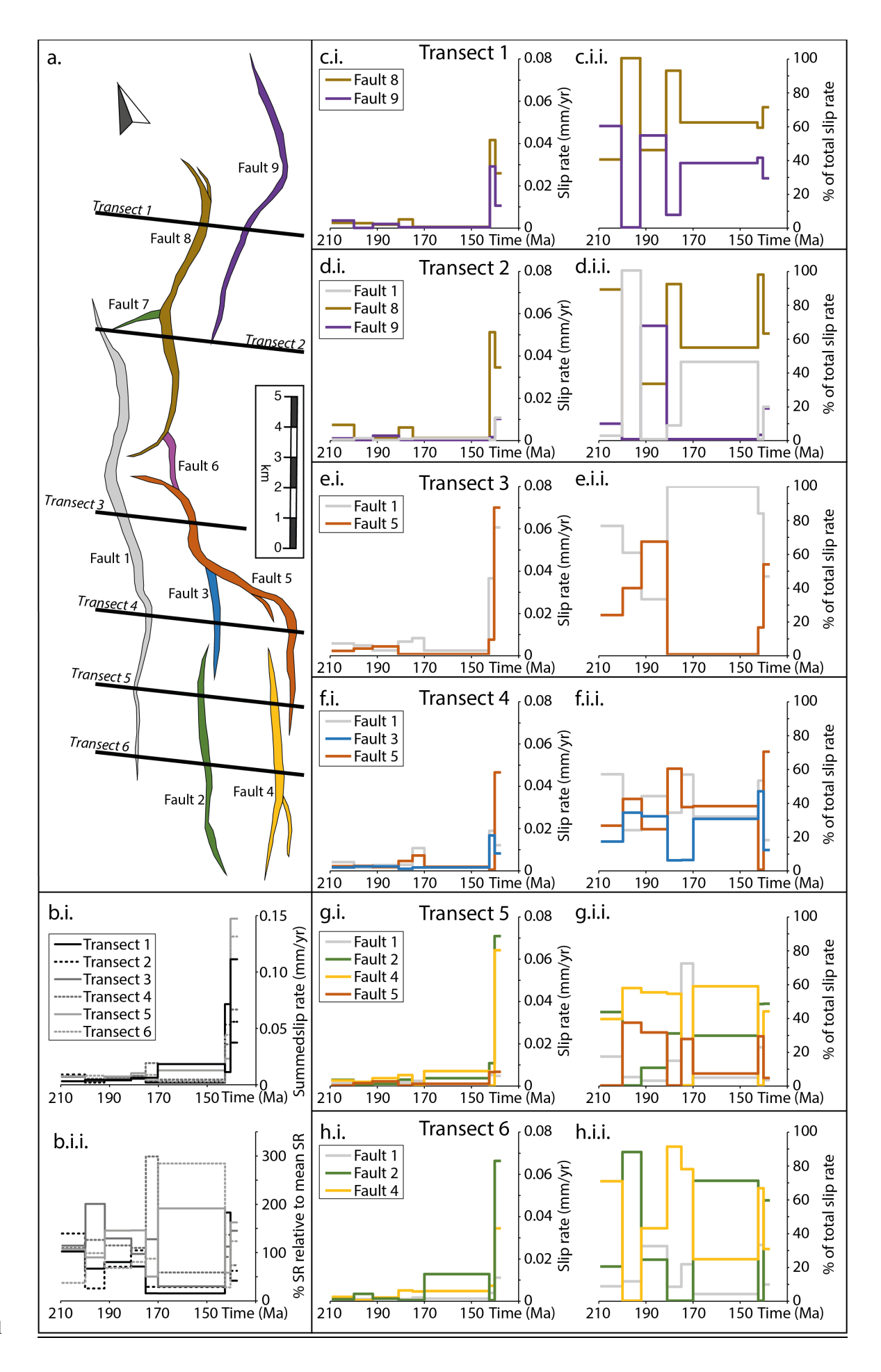


Figure 5 – Slip rate variations across a fault network. a) Fault polygons for the base syn-rift 452 453 horizon showing the locations of the transects taken perpendicular to the overall strike of the fault network. The colour coding of each fault is consistent throughout the figure. b) Cumulative 454 slip rate along each transect (i), calculated by summing the individual slip rates for each fault. 455 This shows the general pattern of the fault network speeding up and slowing down over time. 456 457 The balance of slip rate along-strike of the fault network is shown to vary over time (ii). c-h) Slip rate changes for faults along each individual transect, shown as absolute slip rate values (i) and 458 459 as a percentage of the total slip rate along each transect (ii). Note that the percentage of sliprate taken up on individual faults varies with time, indicating that the relative dominance of 460 faults in this small rift is changing over time. 461

Whereas the magnitude of slip rate varies through time across all transects, another key observation is how the dominance of different faults changes, as seen on all transects (Figure 5c-h, ii). For example, in Transect 1, Fault 8 accommodates the majority (i.e., >50%) of the deformation from 200-192 Ma and 181-137.3 Ma, whereas Fault 9 is dominant from 209.5-200 Ma and 192-181 Ma. A similar pattern can be seen in Transect 3 (the other transect with only two faults across strike), with Fault 1 being dominant from 209.5-192 Ma and 181-140 Ma, and Fault 5 from 192-181 Ma and 140-137.3 Ma. Where there are more than two faults across strike (i.e., all other transects), the patterns of dominance between the faults are more complex, with: (1) faults sharing the extension approximately equally, e.g. Transect 4, 170-142.3 Ma (Figure 5f.i.i.), or (2) two out of three faults taking up the extension, e.g. Transect 2, 181-142.3 Ma, during which time Fault 9 is not slipping (Figure 5dii), or (3) one fault being dominant (e.g. Transect 6, Fault 4 accommodating 70% of extension during 209.5-200 Ma and 92% of extension during 181-175 Ma, with Fault 2 taking-up 92% of extension during 200-192 Ma (Figure 4hii)). This demonstrates that the way that extension is shared across a normal fault network is complex and varies through time, with activity and dominance switching between faults.

4.3 Seismic hazard due to slip rate variations

462 463

464

465

466 467

468 469

470

471

472

473 474

475

476

477

478

479

480

481

482

483 484

485

486 487 The cumulative annual earthquake occurrence rates of individual faults (Fig 6a) and the fault network (Fig S4.2; S4.4) were calculated using fault properties extracted across the full time window (i.e., 209.5 to 137.3), and the four-time intermediate time intervals investigated in this study (Table S3). Similarly to other faults across the Exmouth Plateau (Lathrop et al., 2021), we observe fault length to be established quickly across most faults, and therefore for most faults we use the same fault length for all time intervals. An exception to this is sections of F4, and the tips of F2, that show no slip during the 209.5 to 192 ma time period (Fig 4b, c), suggesting these faults grew between the first two time periods. To account for this, we split F4 into F4a and F4b during the 209.5 to 192 Ma time period and calculate earthquake occurrence

rates for each section separately, while using different lengths of F2 in the first and subsequent time periods. To compare different time windows, recurrence intervals for earthquakes with Mw > 4.0 (Table S4.2) and Mw > 5.0 (Table S4.3) were calculated by taking the inverse of their annual cumulative rates. In this study, we are primarily interested in the variation of the calculated recurrence intervals, rather than the absolute values, because the studied faults studied are presently inactive.

4.3.1 Earthquake rates on Fault 1

For Mw > 5.0 earthquakes on Fault 1, the recurrence interval calculated using rift-averaged slip rate is 27,900 years; however, this differs from recurrence intervals calculated using intermediate horizons (Table S4). Similar recurrence intervals were calculated for the 209.5 to 192 Ma (35,700 years) and 192 to 170 Ma (31,900 years) time periods, before rates increasing by a factor of two during the 170 to 142.3 Ma time period (68,600 years), and decrease by a factor of 10 in the final time period (142.3 to 137.3 Ma, 4,380 years). Similar trends are also observed for Mw > 4.0 earthquakes (Table S4.2). The chosen time window that slip-rate is calculated over therefore has a large effect on recurrence rates. For example, earthquake rates calculated using slip-rate extracted from the 3rd time interval would underestimate the seismic hazard in the following 4th time interval, and the use of time-

average slip-rate could either over-, or under- estimate the recurrence times of damaging
 earthquakes when compared to using rates calculated using intermediate horizons.

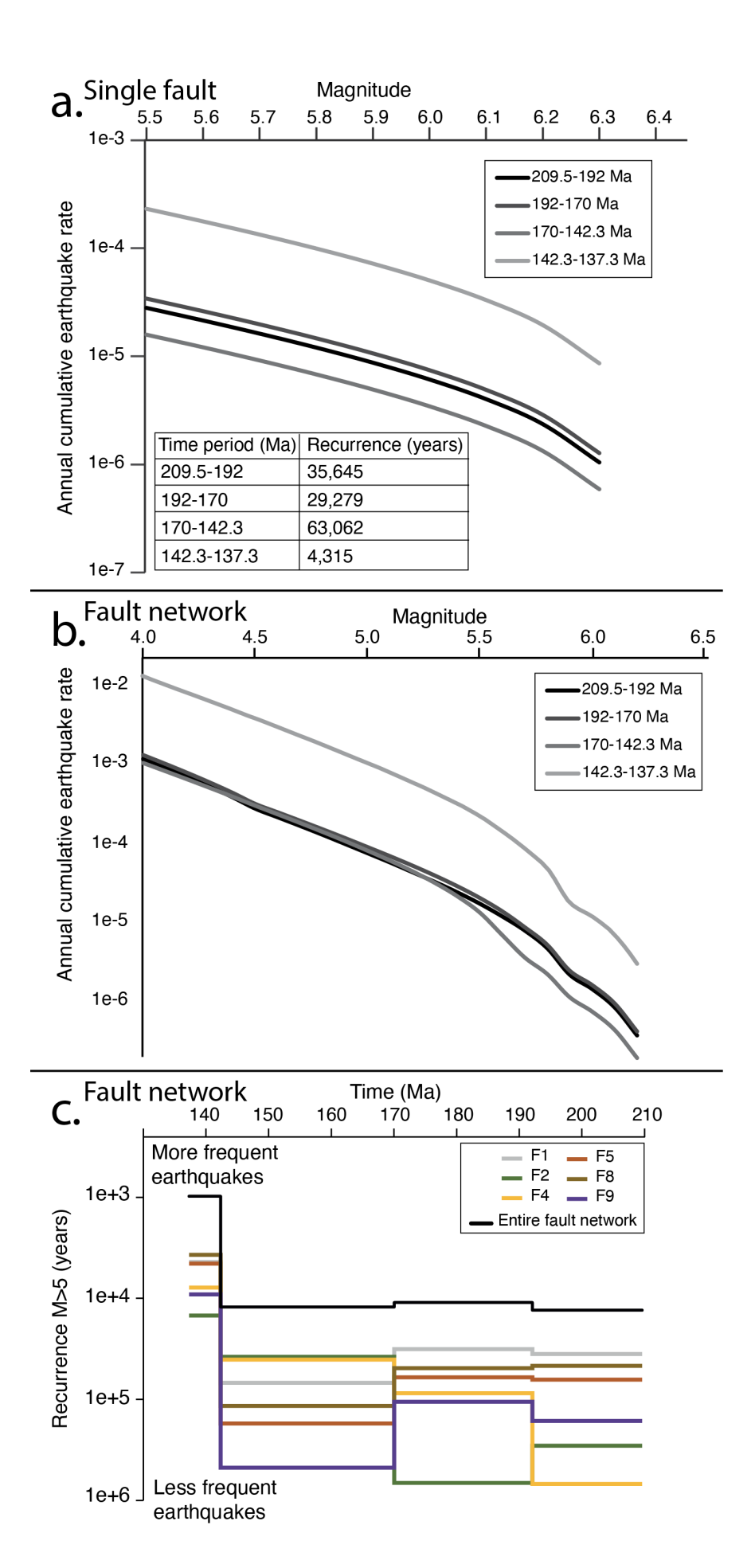


Figure 6 – Seismic hazard calculations utilising variable slip rates. a. Annual cumulative rate of earthquakes for the single fault, using the slip rates derived from different time intervals. The variation in recurrence interval for earthquakes M>5.5 is tabulated. This shows that the order or magnitude variation in slip rate results in an order of magnitude variation in the recurrence interval. b. Annual cumulative rate of earthquakes for the fault network studied, using the slip rates derived from different time intervals. The time interval with the highest slip rate (Figure 4a) has the highest annual cumulative earthquake rate. c. Variation over time in recurrence interval for M>5 earthquakes on individual faults and for the whole fault network. Similar to the proportion of slip rate (Figure 4d), the fault with the highest hazard (i.e. the smallest recurrence interval) varies throughout time. The total hazard across the system also varies with time, similar to the total slip rate across the network (Figure 2b).

4.3.2 Earthquake rates across the fault network

The recurrence time and cumulative earthquake rates across the fault network depend on the time period of interest, and the earthquake magnitude (Fig 6b, c). Similarly to Fault 1, the recurrence interval of M>5 earthquakes calculated using rift averaged slip rates (7,820 years) differs from individual time periods (Table S4), and a reduction in recurrence intervals of M>5 across the fault network from 12,200 to 977 years occurs during the final time period (142.3 to 137.3 Ma; Fig 6b, Table S3-4). During the first three time periods (i.e., 209.5 to 142.3 Ma), the recurrence intervals of M>5 (11,000 to 13,100 years; Table S4) and M>4 (760 to 952 years; Table S3) earthquakes are similar, with the cumulative earthquake rate curves closely spaced at lower magnitudes (Fig 6a, S4.4). However, at magnitudes above 5.5, earthquake rates are lower during the 170 to 142.3 Ma time period, when compared to preceding time periods, coinciding with a deceleration in the three longest faults in the network (F5, F8, F9; Table S2).

Where the recurrence rates on individual faults are considered, recurrence rates show a high degree of variation between time intervals (Figure 6c, Fig S4.1, Table S4.2-S4.3), even where rates across the whole network remain similar (Fig 6c). For example, comparing the 209.5 to 192 Ma time period, where recurrence rates of M>5.0 earthquakes are 13,100 years, to the 170 to 142.3 Ma time period, where recurrence rates across the network are 12,200 years, the difference in rates between time windows on individual faults range from 32,900 years (F1) to 649,000 years (F4). These differences mean that the contribution of earthquake rates differ across the network, depending on the fault and time period. Some faults contribute similarly to the earthquake rate across different time periods, for example Fault 1 which contributes 28% to the cumulate rate of M>5.0 earthquakes using the rift averaged slip-rate and between 18% (170 to 142.3 Ma) and 37% (209.5 Ma to 192 Ma) using intermediate time windows. Conversely, some faults such as Fault 4 vary considerably between time periods,

which contributes 9% to the cumulate rate of M>5.0 earthquake using the rift averaged slip-rate, but ranges from 2% (209.5 to 192 Ma) to 32% (170 to 142.3 Ma).

In addition to slip-rate, fault length also affects how earthquake rates are distributed across the fault network (Table S4.2, S4.2, S4.4). Firstly, three of the studied faults were too small to generate M>5 earthquakes (Faults 3, 6, 7; Table S4.1, Fig S4.4), and therefore the effect of these faults is only observed when recurrence rates of M>4.0 earthquakes are considered (Fig S4.1). Whilst Faults 3 and 6 contribute similarly to the fault network across all time periods (1 to 4% and 1 to 2% respectively), Fault 7 contributes 21% for M>4.0 earthquakes during the first two time periods, before dropping to 4% in 170 to 142.3, and 1% in 142.3 to 137.3 Ma. This highlights that although similar patterns are observed for M>4.0 earthquakes, the relative proportion across the network is not identical to M>5.0, and different faults can contribute more to the recurrence rates of different magnitude earthquakes (Fig S4.4. Table S4.2, S 4.3). Where slip-rate decreases on a longer fault (e.g., Fault 5), this will have a greater impact on M>5 earthquakes when compared to changes in slip-rate on shorter faults (e.g., Fault 2). Additionally, where a fault lengthens between time intervals (e.g., Fault 4), the recurrence time of larger earthquakes can decrease, even where the change in slip-rate across these time intervals is limited (Table S4.1). Therefore, both the spatial distribution and frequency of damaging earthquakes (M>5.0) across the network can vary through time depending on the distribution of slip-rate across the network, and the length of the faults which accommodate the majority of the slip during a given time period.

5 Discussion and implications

543544

545

546

547548

549550

551552

553554

555556

557558

559

560

561

562

563

564

565

566567

568

569

570571

572

573

574

575

576

577

5.1 Temporal slip rate variability

Our data reveals temporal variability in slip rates across individual faults and the fault network (Figs 3, 4, 5). Although the absolute slip rates are relatively low when compared to those in global compilations (Nicol et al., 1997), they are consistent with slip rates extracted from other normal faults on the NW Shelf of Australia (Andrews et al., 2024; Lathrop et al., 2021; Pan et al., 2022). Despite being relatively low, slip-rates across the study area vary by up to an order of magnitude across the studied time period (Figs 3-5), suggesting temporal slip-rate variability should be considered when reconstructing fault histories.

Slip-rate variations are observed across a diverse range of tectonic settings and time periods (e.g., Dolan et al., 2007b; Friedrich et al., 2003; Gauriau & Dolan, 2021; McClymont et al., 2009; Nicol et al., 2016). Comparing these variations across different faults and tectonic settings requires a consistent metric. A common value for quantifying earthquake variability in seismic hazard studies is the Coefficient of Variation (CV, the standard deviation of recurrence times divided by the mean recurrence time). However, faults with different slip histories can

578

579

580

581 582

583

584

585

586

587

588

589

590

591

592

593 594

595

596

597

598 599

600

yield identical CVs, since the metric captures only the variability on the recurrence intervals and not the sequence of events nor the magnitude of slip (Cowie et al., 2012). They proposed a measure of slip-rate variability by calculating the ratio between the standard deviation of slip rate over a sliding time window to the mean slip rate. Although this metric is argued by the authors to be a more robust indicator of variability in slip histories, it requires a continuous sliphistory, which is often unavailable due to non-uniform time windows over which slip rates are calculated (e.g., Lathrop et al., 2021; Meyer et al., 2002; Nixon et al., 2024; Weldon et al., 2004). Gauriau and Dolan (2021) suggested calculating slip-rate variability by dividing the fastest slip-rate by the slowest, but this returns very high values for intercontinental faults with large differences between maximum and minimum rates, or infinite values of slip-rate variability for faults with periods of quiescence (Table S6.1). This makes comparing variability between faults across different tectonic settings challenging. To overcome these limitations, we introduce a new measure, termed the normalised slip-rate variability (NSRV), defined as the range (maximum rate – minimum rate) in slip-rate divided by the slip-rate averaged over the studied time interval (i.e. total slip divided by total time, which is thousands to millions of years). NSRV offers a simple yet robust metric for quantifying slip-rate variability in diverse geological contexts.

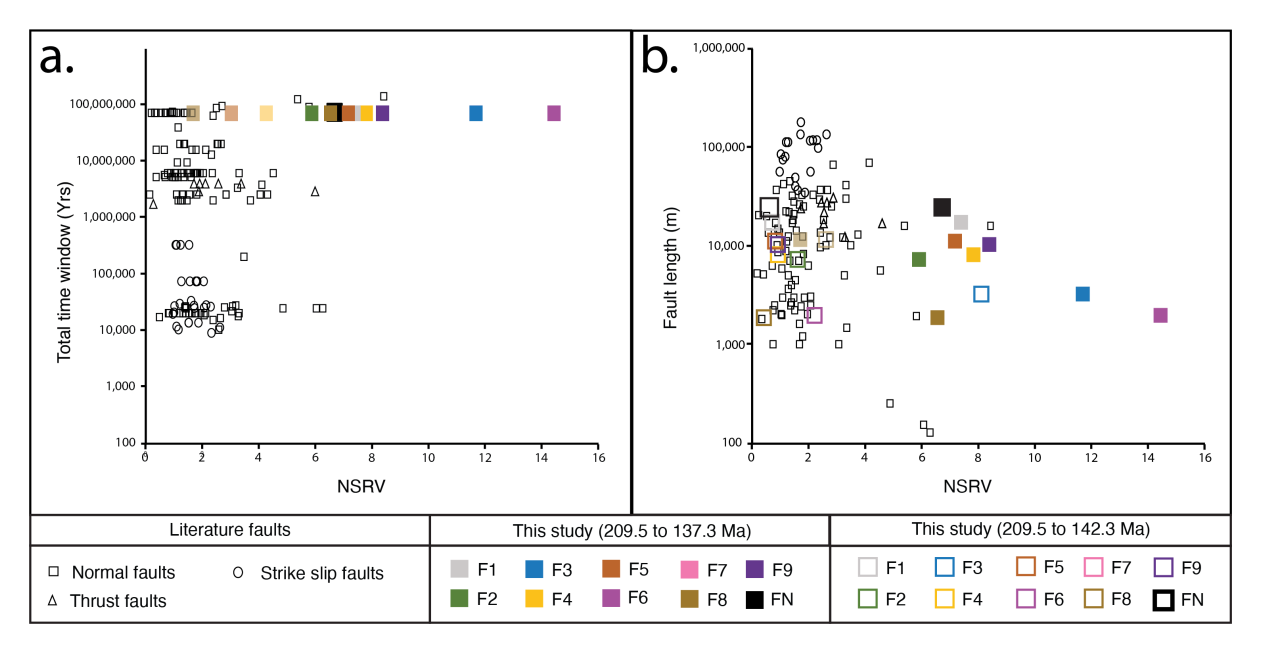


Figure 7: Normalised slip-rate variability (NSRV) calculated for the studied faults and a compilation of normal (n = 108), strike-slip (n = 27) and thrust (n = 8) faults that show incremental variations in slip-rate across their growth histories. NSRV is plotted against the a) total time period that slip-rate is investigated over and b) fault length. Data from this study is colour coded by fault, faults splay data are shown in the same colour with transparency

- applied. When the last time period (142.3-137.3Ma) is omitted from calculating the NSRV, all values are lower (Table S6.3) and are plotted on b) for comparison.
- 603 We compiled incremental slip histories for time periods >10 kyrs (i.e. covering multiple seismic
- 604 cycles) for 151 faults from the literature and this study, and calculated their corresponding
- 605 normalised slip-rate variability (NSRV) (Fig 7, Table S6.4). For individual faults in our study, NSRV
- values range from 1.7 to 14.4 (average = 7.1), with the whole fault network having a value of
- 6.7 (Table S6.2). This is notably higher than most published examples (range = 0.8 to 8.4,
- average = 1.9). The elevated NSRV from our study is partly driven by a rapid acceleration in slip
- 609 rate across the network during the final time period considered (i.e. between 142.3 and 137.3
- 610 Ma, Fig 5). However, if we disregard the final time period (Figure 7b; Table S6.3), NSRV across
- 611 the full network is low (NSRV = 0.6); although individual faults still show a wide range in NSRV
- values (NSRV = 0.4 to 8.1, Average = 1.9). This is because the proportion of slip accommodated
- by a particular fault during a specific time period does not remain constant (Fig 4, 5), causing a
- large range between maximum and minimum slip-rates and therefore a high NSRV. This
- 615 highlights that, like in active systems such as the Central Apennines (Faure Walker et al., 2012;
- Pesci et al., 2009), temporal variations in strain accommodation on individual faults can occur
- even where the strain across the network remains constant.
- Analysis of the global dataset reveals that NSRV is largely unaffected by the duration over which
- it is measured, with faults that have been active for < 1 Ma having an average NSRV of 1.8,
- whereas those > 1 Ma averaging 2.0. Fault length does not appear to influence NSRV, with a
- 621 wide NSRV range of values being observed across both long and short faults (Fig 7b). However,
- NSRV differs by fault type, with normal faults showing higher NSRV (2.0, n = 116) compared to
- strike-slip faults (1.4, n = 27), although there is insufficient data to assess thrust faults (2.5, n =
- 8). The consistently high NSRV values across timescales and fault lengths suggests slip-rate
- 625 variability is an intrinsic feature of fault growth, with normal faults exhibiting particularly
- 626 irregular behaviour.
- Several mechanisms have been proposed to explain long-term (million-year) changes in slip-
- rate on normal faults, including strain localisation onto border faults during rift evolution
- 629 (Meyer et al., 2002; Nixon et al., 2024; Walsh et al., 2003), variable plate velocities (Andrew
- 630 Nicol et al., 2005), and incremental slip rate due to fault-segment linkage (Cartwright &
- Mansfield, 1998; Cartwright et al., 1995) Our study area, which is <20 km wide, does not image
- border faults and shows no evidence for localisation onto larger faults over the studied time
- period, with slip accrued on all faults across all time periods (Figure 4). Although changes in
- 634 plate velocity are difficult to constrain across the NW Shelf due to only half the margin being
- preserved (Lathrop et al., 2021), no regional change has been suggested that would explain the
- 636 timing and magnitude of the observed slip-rate acceleration between 142.3 and 137.3 Ma (Bilal

& McClay, 2022). Along-strike segment linkage is known to influence slip-rates during the early stages of fault growth (Meyer et al., 2002; Nixon et al., 2024). However, our slip profiles show that, similar to elsewhere on the Exmouth Plateau (Lathrop et al., 2021; Pan et al., 2022), all faults, except Fault 4, followed the constant length model of fault growth (Childs et al., 2017; Rotevatn et al., 2019), reaching their maximum length during the 209.5 to 192 Ma time window, and thus we assumed a constant fault length for the seismic hazard calculations. We propose that fault network geometry, i.e. the proximity and spacing of faults, appears to affect slip-rates of individual faults in the study area (Figure 4, 5) as discussed further below.

5.2 The influence of fault network geometry on spatial-temporal slip rate variability

637 638

639 640

641

642

643

644

645

646 647

648

649

650651

652

653

654

655

656

657658

659 660

661

662

663

664

665 666

667 668

669

670671

672

Our data shows that the location of maximum slip-rate on individual faults (Fig 3, 4), and the proportion of slip accommodation on individual faults (Fig 5) varies through time, supporting hypothesis 2 for both research questions posed (How does displacement accumulate along a single fault over time? How does displacement accumulated across a fault network over time? (Figure 1). This agrees with individual fault behaviour observed from physical analogue (Mansfield & Cartwright, 2001; Schlagenhauf et al., 2008) and numerical (Cowie et al., 2012) models of fault network growth. However, the summed slip-rate profile is more supportive of hypothesis 1 (Fig 4), with the position of maximum slip-rate being fixed near the centre of the fault, apart from between 170 Ma and 142.3 Ma, when a southwards shift of ~5km occurs due to an increase in the slip rates of Faults 2 and 4 (Fig 4d). This suggests that while the distribution of strain across the network remains consistent, how that strain is partitioned between faults varies between time periods. Similar observations of faults accommodating variable proportions of displacement have been documented in the Italian Apennines and central Greece for much shorter timescales, where cosmogenic dating reveals spatial-temporal slip-rate changes during the last 15 kyr (Benedetti et al., 2013; Cowie et al., 2017; lezzi et al., 2021; Mildon et al., 2022; G. P. Roberts et al., 2024, 2025; Sgambato et al., 2025). Over this 15 kyr timescale, regional strain in the Apennines is assumed to have remained stable (Faure Walker et al., 2012), with stress transfer between faults and underlying shear zones invoked as the cause of slip-rate changes (Mildon et al., 2022). It is unlikely that the physical mechanisms hypothesised for central Italy are applicable to our dataset, given the difference in timescales and length scales. However, these observations highlight the need to account for both the growth of individual faults and the overall distribution of strain when assessing fault network evolution.

Fault interactions play a key role in the distribution and evolution of slip on faults within a fault network by producing local stress concentrations and perturbations that affect the geometry, kinematics, and earthquake rupture patterns of interacting faults (e.g., (H. Fossen et al., 2005; Kattenhorn et al., 2000; Nixon et al., 2014; Peacock et al., 2017; Rodriguez Piceda et

al., 2025). Interactions can occur on geometrically linked faults, which are physically connected by a branch line, and/or kinematically linked, where slip patterns on two or more faults are complimentary (Nixon et al., 2014; Peacock et al., 2017). The network studied herein shows a combination of both interaction types (Fig 4ai), with the arrangements of faults having a direct effect on slip accumulation. We find greater variability in the proportion of slip on individual faults where multiple faults are arranged across-strike (e.g., Transects 4-6; Figure 5f-h). Even where only two across-strike faults are present, strain and stress transfer occurs (e.g., Figure 5c). Similar patterns, though over very different spatial scales, have been documented in the Italian Apennines, where less variability is observed in the Southern Apennines in a location where faults are predominantly arranged along-strike from each other, when compared to the Central Apennines, where faults are predominantly arranged across strike. At the millennial scale of the earthquake cycle, across-strike faults are known to exhibit complex slip behaviours, including partial ruptures, slow-slip events, and earthquake arrest (Mia et al., 2024; Romanet et al., 2018; Yin et al., 2023), with across-strike offsets having a greater effect when compared to along-strike geometries (Rodriguez Piceda et al., 2025). While our slip-rate values cover multiple earthquake cycles, our data suggests that overlapping across-strike fault geometries can continue to influence slip-rate variability over substantially longer million year timescales.

Consistent with previous studies (e.g., Cowie et al., 2012; Gauriau & Dolan, 2021), our findings underscore the role of structural complexity in driving slip-rate variations across multiple time scales. We find greater NSRV values for normal faults, which form as part of faults networks within continental rifts (Fig 7). Rift systems are characterised by many faults arranged in an across-strike geometry (e.g., (Duffy et al., 2017; Scholz & Contreras, 1998)), promoting stress interactions between faults and complex earthquake behaviour (Rodriguez Piceda et al., 2025). Conversely, strike-slip faults are predominantly arranged in an along-strike arrangement, with slip occurring roughly parallel to fault strike (e.g., (Sylvester, 1988; Woodcock, 1986) and thrust faults often localise onto discrete slip planes at a low angle to the compression direction (e.g., (Ellis & Dunlap, 1988). In these cases, stress interactions will be lower and have a different pattern, although not absent particularly in areas of variable fault and fault network geometries (Lin & Stein, 2004; Peacock et al., 2017). The arrangement of normal faults likely explains the higher NSRV values for normal faults (Fig 7), and why areas of continental extension display such variable slip-rates when compared to other plate boundary systems. Overall, our results reinforce the need to consider fault network geometry, and the effect this may have on fault

interactions, when evaluating fault growth and suggest that seismic hazard models that do not consider the whole network may miss critical dynamics inherent to fault networks.

5.3 Implications of slip rate variability for seismic hazard assessment

705

706

707

708

709

710

711

712

713

714715

716

717

718719

720

721

722

723724

725

726

727

728

729

730

731732

733734

735

736

737738

Active fault systems are characterised by temporal variations in slip-rate variability (lezzi et al., 2020; McClymont et al., 2009; Nixon et al., 2024; Roberts et al., 2024, 2025; Sgambato et al., 2025), leading to corresponding variations in earthquake recurrence, and thus highlighting the need for time-dependent seismic hazard assessments (Dahm & Hainzl, 2022; Verdecchia et al., 2019). In our study, slip-rates fall in the lower end of the expected range for normal faults relative to known faults and their slip rates (Nicol et al., 1997), leading to recurrence intervals for Mw > 5 earthquakes of ~4,000 to ~63,000 years on the single fault, substantially longer than the hundreds to thousands of years typically observed in actively extending regions (e.g. Greece, central Italy, Basin and Range, USA (Console et al., 2013; Galli, 2020; Schwartz & Coppersmith, 1984)). Despite this, the magnitude of slip-rate variability from our study is comparable to other active extensional systems (Figure 7 for comparison). Probabilistic Seismic Hazard Assessment (PSHA) typically relies on single, time-averaged slip-rates derived from geological data (e.g., Pace et al., 2016; Williams et al., 2023), which can include some temporal variations in slip rate, but which do not fully explore their impact. Where time-dependence is incorporated, usually through Coulomb stress modelling, it often relies on short historical and/or instrumental records (e.g., Chan et al., 2017; Dahm & Hainzl, 2022; Toda et al., 1998; Verdecchia et al., 2019). Both data types have limitations: geological records rarely resolve long-term (>100 kyr) variability (Cowie et al., 2012), while instrumental and historical datasets are often too short and incomplete to span full seismic cycles (Mäntyniemi et al., 2014; Swafford & Stein, 2007). By comparing slip-rates calculated across multiple time windows (Figure 4, 5), we show how the width of the time window will affect earthquake rates. For example, on Transect 3, slip acceleration initiates during the 142.3-140 Ma interval and intensifies during the 140–137.3 Ma interval. Averaging across the full 142.3–137.3 Ma window would therefore overestimate hazard in the earlier part of the interval and underestimate it in the latter. This demonstrates that slip-rate inputs must be derived from time windows long enough to capture clustered or transient behaviour (e.g., Friedrich et al., 2003), yet not so long that they obscure meaningful long-term variability. Although driven by different mechanisms, this behaviour mirrors evidence from active systems such as the Corinth Rift in Greece, where fault linkage and localisation onto major structures are associated with fault-specific slip rates over the past 2 Myr, with significant changes occurring as recently as 130 ka (Nixon et al., 2024). Our findings reinforce the importance of characterising slip-rate variability across

relevant timescales and quantifying the uncertainty introduced when long-term rates do not reflect present-day fault behaviour.

739

740

741

742

743

744

745

746

747748

749750

751

752

753754

755 756

757

758

759

760

761762

763764

765

766

767 768

769

In addition to temporal changes in recurrence rates, the spatial distribution of hazard also varies as different faults in the system accommodate strain at different times. Although the total rate of Mw > 5 earthquakes across the network remains similar up to 142.3 Ma (~10,000 years, Figure 6c), the rates on individual faults differ. For instance, Fault 9 has the highest Mw > 5 earthquake rates between 192 and 209.5 Ma, whereas Faults 2 and 4 became more active later, between 142.3 and 170 Ma. This southward migration of elevated earthquake rates by > 10 km illustrates that changes in fault-specific slip rates can alter the rates of damaging earthquakes at a specific location, even if regional strain rates remain constant. Similar behaviour is observed in active regions such as the Central Apennines, where slip-rate variability is spatially complex, especially where multiple faults are arranged across strike from each other (Roberts et al., 2024; Rodriguez Piceda et al., 2025; Sgambato et al., 2023). This suggests that time-dependant PSHA needs to consider not only short term factors that cause earthquake clustering, but also how the long-term slip rate behaviour of faults within the network may evolve differently. One way to address this is by testing the effects of the spatiotemporal variability of long-term slip-rate on earthquakes rates with physics-based earthquake simulators (e.g. Herrero-Barbero et al., 2023; Shaw et al., 2018).

In addition to changes in absolute slip-rate, we observe changes in the shape of slip-rate profiles between faults and time periods. Faure Walker et al. (2019) show that spatially variable slip rate and, specifically, assumptions about the slip rate profile shape (e.g., triangular vs. boxcar) can alter calculated strain rates by a factor of 0.5 to 1.5 and change calculated earthquake occurrence rates by 100s of years (from 262-524 years in their published example). In our analysis, the overall network slip-rate profile is similar in three of the four main time intervals (Figure 4bii, cii, eii), but it differs markedly during 170 to 142.3 Ma (Figure 4dii). At the level of an individual fault, displacement profiles exhibit large variation in shape, including multiple peaks and troughs (Figure 4). This contrast with the smoother, time-average slip rate profile (e.g., Figure 4aii). As a result, estimates of earthquake rates using the "time-averaged" slip-rate profile could diverge significantly from those derived using the slip-rate profiles of individual faults (Figure 4b-e). These findings highlight the potential limitations of spatial and temporal averaging and underscore the importance of incorporating fault-specific, time-

dependent slip-rate variability into seismic hazard models, particularly in fault networks containing multiple faults arranged across-strike from each other.

5 Conclusions

In this study, we used high-resolution 3D seismic reflection data to quantify how slip rates evolve along and across a network of normal faults over a ~70 Myrs. Our results reveal substantial spatial and temporal variability in slip rate, even on faults with relatively simple geometries. Along-strike slip-rate profiles change shape through time, and rates can vary by up to two orders of magnitude, indicating that single-point measurements may underrepresent the complexity of fault behaviour. Across the fault network, slip is not consistently partitioned, with different faults dominating at different time periods and the location of maximum slip changing through time. These patterns suggest that fault interactions and network geometry play a key role in controlling the distribution of strain within a fault network at million-year timescales.

By calculating earthquake recurrence rates, we find that the summed rates of Mw >5 earthquakes remained consistent across the first three time periods, prior to reducing by reducing by an order of magnitude to ~1000 years during the 142.3 to 137.3 Ma time period. We find that while summed rates may remain consistent, the contributions from individual faults vary markedly between time intervals. By considering which faults are contributing to the summed rates, the dominant faults move from the north to the south of the fault network. This highlights that the spatial distribution of large earthquakes could differ between different time periods. Our study demonstrates the importance of considering fault network geometry when undertaking seismic hazard assessments or building tectonic models.

Acknowledgments

- We would like to thank DugInsight for the provision of an academic license for their software
- package. We thank Francesco Visini for his help to begin the FiSH modelling. This work was
- supported by a UKRI Future Leaders Fellowship MR/ T041994/1 (PI Z. Mildon).

Conflict of Interest Disclosure

"The authors declare there are no conflicts of interest for this manuscript."

References

- Alcalde, J., Bond, C. E., Johnson, G., Ellis, J. F., & Butler, R. W. H. (2017). Impact of seismic image
- quality on fault interpretation uncertainty. GSA Today. https://doi.org/10.1130/GSATG282A.1

- Allen, P. A., & Allen, J. R. (2013). Basin Analysis: Principles and Application to Petroleum Play
- 802 Assessment. John Wiley & Sons.
- Andrews, B. J., Mildon, Z. K., Jackson, C. A. L., & Bond, C. E. (2024). Quantifying fault
- interpretation uncertainties and their impact on fault seal and seismic hazard analysis. Journal
- of Structural Geology, 184, 105158. https://doi.org/10.1016/j.jsg.2024.105158
- Barrett, B. J., Hodgson, D. M., Jackson, C. A. -L., Lloyd, C., Casagrande, J., & Collier, R. E. Ll.
- 807 (2021). Quantitative analysis of a footwall-scarp degradation complex and syn-rift stratigraphic
- architecture, Exmouth Plateau, NW Shelf, offshore Australia. Basin Research, 33(2), 1135–1169.
- 809 https://doi.org/10.1111/bre.12508
- Benedetti, L., Finkel, R., Papanastassiou, D., King, G., Armijo, R., Ryerson, F., et al. (2002). Post-
- glacial slip history of the Sparta fault (Greece) determined by 36Cl cosmogenic dating: Evidence
- for non-periodic earthquakes. Geophysical Research Letters, 29(8), 87-1-87–4.
- 813 https://doi.org/10.1029/2001GL014510
- Benedetti, L., Manighetti, I., Gaudemer, Y., Finkel, R., Malavieille, J., Pou, K., et al. (2013).
- 815 Earthquake synchrony and clustering on Fucino faults (Central Italy) as revealed from in situ
- 36Cl exposure dating. Journal of Geophysical Research: Solid Earth, 118(9), 4948–4974.
- 817 https://doi.org/10.1002/jgrb.50299
- 818 Bilal, A., & McClay, K. (2022). Tectonic and stratigraphic evolution of the central Exmouth
- Plateau, NW Shelf of Australia. Marine and Petroleum Geology, 136.
- 820 https://doi.org/10.1016/j.marpetgeo.2021.105447
- Bilal, A., McClay, K., & Scarselli, N. (2020). Fault-scarp degradation in the central Exmouth
- Plateau, North West Shelf, Australia. Geological Society, London, Special Publications, 476(1),
- 823 231–257. https://doi.org/10.1144/SP476.11
- 824 Black, M., McCormack, K. D., Elders, C., & Robertson, D. (2017). Extensional fault evolution
- within the Exmouth Sub-basin, North West Shelf, Australia. Marine and Petroleum Geology, 85,
- 826 301–315. https://doi.org/10.1016/j.marpetgeo.2017.05.022
- 827 Bond, C. E. (2015). Uncertainty in structural interpretation: Lessons to be learnt. Journal of
- 828 Structural Geology, 74, 185–200. https://doi.org/10.1016/j.jsg.2015.03.003
- 829 Brown, A. R. (2011). Interpretation of Three-Dimensional Seismic Data (7th ed.). American
- 830 Association of Petroleum Geologists.

- 831 Brune, J. N. (1968). Seismic moment, seismicity, and rate of slip along major fault zones. Journal
- of Geophysical Research (1896-1977), 73(2), 777–784.
- 833 https://doi.org/10.1029/JB073i002p00777
- Cartwright, J. A., & Mansfield, C. S. (1998). Lateral displacement variation and lateral tip
- geometry of normal faults in the Canyonlands National Park, Utah. Journal of Structural
- 836 Geology, 20(1), 3–19. https://doi.org/10.1016/S0191-8141(97)00079-5
- 837 Cartwright, Joseph A., Trudgill, B. D., & Mansfield, C. S. (1995). Fault growth by segment linkage:
- an explanation for scatter in maximum displacement and trace length data from the
- Canyonlands Grabens of SE Utah. Journal of Structural Geology, 17(9), 1319–1326.
- 840 https://doi.org/10.1016/0191-8141(95)00033-A
- 841 Chan, C., Wang, Y., Wang, Y., & Lee, Y. (2017). Seismic-Hazard Assessment over Time: Modeling
- Earthquakes in Taiwan. Bulletin of the Seismological Society of America, 107(5), 2342–2352.
- 843 https://doi.org/10.1785/0120160278
- Chartier, T., Scotti, O., & Lyon-Caen, H. (2019). SHERIFS: Open-Source Code for Computing
- 845 Earthquake Rates in Fault Systems and Constructing Hazard Models. Seismological Research
- 846 Letters, 90(4), 1678–1688. https://doi.org/10.1785/0220180332
- Chellingsworth, L., Bentley, M., & Wynn, T. (2015). Human factors in seismic uncertainty —
- Restoring a realistic uncertainty range. Interpretation, 3, SQ21–SQ32.
- 849 https://doi.org/10.1190/INT-2014-0203.1
- 850 Childs, C., Holdsworth, R. E., Jackson, C. A.-L., Manzocchi, T., Walsh, J. J., & Yielding, G. (2017).
- 851 Introduction to the geometry and growth of normal faults. In C. Childs, R. E. Holdsworth, C. A.-L.
- Jackson, T. Manzocchi, J. J. Walsh, & G. Yielding (Eds.), The Geometry and Growth of Normal
- Faults (Vol. 439, p. 0). The Geological Society of London. https://doi.org/10.1144/SP439.24
- 854 Childs, Conrad, Worthington, R. P., Walsh, J. J., & Roche, V. (2019). Conjugate relay zones:
- geometry of displacement transfer between opposed-dipping normal faults. Journal of
- 856 Structural Geology, 118, 377–390. https://doi.org/10.1016/j.jsg.2018.11.007
- 857 Console, R., Falcone, G., Karakostas, V., Murru, M., Papadimitriou, E., & Rhoades, D. (2013).
- 858 Renewal models and coseismic stress transfer in the Corinth Gulf, Greece, fault system. Journal
- of Geophysical Research: Solid Earth, 118(7), 3655–3673. https://doi.org/10.1002/jgrb.50277
- 860 Cowie, P. A., & Scholz, C. H. (1992). Growth of faults by accumulation of seismic slip. Journal of
- 861 Geophysical Research, 97(B7), 11085–11095.

- 862 Cowie, P. A., Underhill, J. R., Behn, M. D., Lin, J., & Gill, C. E. (2005). Spatio-temporal evolution
- 863 of strain accumulation derived from multi-scale observations of Late Jurassic rifting in the
- 864 northern North Sea: A critical test of models for lithospheric extension. Earth and Planetary
- 865 Science Letters, 234(3), 401–419. https://doi.org/10.1016/j.epsl.2005.01.039
- Cowie, P. A., Roberts, G. P., Bull, J. M., & Visini, F. (2012). Relationships between fault
- geometry, slip rate variability and earthquake recurrence in extensional settings: Fault
- geometry control on earthquake rupture. Geophysical Journal International, 189(1), 143–160.
- 869 https://doi.org/10.1111/j.1365-246X.2012.05378.x
- 870 Cowie, P. A., Phillips, R. J., Roberts, G. P., McCaffrey, K., Zijerveld, L. J. J., Gregory, L. C., et al.
- 871 (2017). Orogen-scale uplift in the central Italian Apennines drives episodic behaviour of
- earthquake faults. Scientific Reports, 7(1), 44858. https://doi.org/10.1038/srep44858
- Dahm, T., & Hainzl, S. (2022). A Coulomb Stress Response Model for Time-Dependent
- Earthquake Forecasts. Journal of Geophysical Research: Solid Earth, 127(9), e2022JB024443.
- 875 https://doi.org/10.1029/2022JB024443
- 876 Delogkos, E., Sagab, M. M., Walsh, J. J., Roche, V., & Childs, C. (2020). Throw variations and
- strain partitioning associated with fault-bend folding along normal faults. Solid Earth, 11(3),
- 878 935–945. https://doi.org/10.5194/se-11-935-2020
- Deng, H., & McClay, K. (2019). Development of extensional fault and fold system: Insights from
- 880 3D seismic interpretation of the Enderby Terrace, NW Shelf of Australia. Marine and Petroleum
- 881 Geology, 104, 11–28. https://doi.org/10.1016/j.marpetgeo.2019.03.003
- Deng, H., & McClay, K. (2021). Three-dimensional geometry and growth of a basement-involved
- fault network developed during multiphase extension, Enderby Terrace, North West Shelf of
- 884 Australia. GSA Bulletin, 133(9–10), 2051–2078. https://doi.org/10.1130/B35779.1
- Direen, N. G., Stagg, H. M. J., Symonds, P. A., & Colwell, J. B. (2008). Architecture of volcanic
- rifted margins: new insights from the Exmouth Gascoyne margin, Western Australia.
- 887 Australian Journal of Earth Sciences, 55(3), 341–363.
- 888 https://doi.org/10.1080/08120090701769472
- 889 Dolan, J. F., Bowman, D. D., & Sammis, C. G. (2007a). Long-range and long-term fault
- interactions in Southern California. Geology, 35(9), 855–858.
- 891 https://doi.org/10.1130/G23789A.1

- 892 Dolan, J. F., Bowman, D. D., & Sammis, C. G. (2007b). Long-range and long-term fault
- interactions in Southern California. Geology, 35(9), 855–858.
- 894 https://doi.org/10.1130/G23789A.1
- Dolan, J. F., McAuliffe, L. J., Rhodes, E. J., McGill, S. F., & Zinke, R. (2016). Extreme multi-
- millennial slip rate variations on the Garlock fault, California: Strain super-cycles, potentially
- time-variable fault strength, and implications for system-level earthquake occurrence. Earth
- and Planetary Science Letters, 446, 123–136. https://doi.org/10.1016/j.epsl.2016.04.011
- 899 Duffy, O. B., Nixon, C. W., Bell, R. E., Jackson, C. A.-L., Gawthorpe, R. L., Sanderson, D. J., &
- Whipp, P. S. (2017). The topology of evolving rift fault networks: Single-phase vs multi-phase
- 901 rifts. Journal of Structural Geology, 96, 192–202. https://doi.org/10.1016/j.jsg.2017.02.001
- 902 Ellis, M. A., & Dunlap, W. J. (1988). Displacement variation along thrust faults: implications for
- the development of large faults. Journal of Structural Geology, 10(2), 183–192.
- 904 https://doi.org/10.1016/0191-8141(88)90115-0
- Etheridge, M. A., & O'Brien, G. W. (1994). Structural and Tectonic Evolution of the Western
- 906 Australian Margin Basin System. Retrieved from
- 907 https://archives.datapages.com/data/petroleum-exploration-society-of-
- 908 australia/journal/022/022001/pdfs/45.htm
- Faleide, T. S., Braathen, A., Lecomte, I., Mulrooney, M. J., Midtkandal, I., Bugge, A. J., & Planke,
- 910 S. (2021). Impacts of seismic resolution on fault interpretation: Insights from seismic modelling.
- 911 Tectonophysics, 816, 229008. https://doi.org/10.1016/j.tecto.2021.229008
- Faure Walker, J. P., Roberts, G. P., Cowie, P. A., Papanikolaou, I. D., Sammonds, P. R., Michetti,
- 913 A. M., & Phillips, R. J. (2009). Horizontal strain-rates and throw-rates across breached relay
- 2014 zones, central Italy: Implications for the preservation of throw deficits at points of normal fault
- 915 linkage. Journal of Structural Geology, 31(10), 1145–1160.
- 916 https://doi.org/10.1016/j.jsg.2009.06.011
- Faure Walker, J. P., Roberts, G. P., Sammonds, P., & Cowie, P. A. (2010). Comparison of
- earthquake strains over 102 and 104 year timescales: Insights into variability in the seismic
- cycle in the central Apennines, Italy. Journal of Geophysical Research: Solid Earth, 115(B10).
- 920 https://doi.org/10.1029/2009JB006462
- 921 Faure Walker, J. P., Roberts, G. P., Cowie, P. A., Papanikolaou, I., Michetti, A. M., Sammonds, P.,
- et al. (2012). Relationship between topography, rates of extension and mantle dynamics in the

- 923 actively-extending Italian Apennines. Earth and Planetary Science Letters, 325–326, 76–84.
- 924 https://doi.org/10.1016/j.epsl.2012.01.028
- 925 Faure Walker, J. P., Visini, F., Roberts, G. P., Galasso, C., McCaffrey, K., & Mildon, Z. (2019).
- Variable fault geometry suggests detailed fault-slip-rate profiles and geometries are needed for
- fault-based probabilistic seismic hazard assessment (PSHA). Bulletin of the Seismological
- 928 Society of America, 109(1). https://doi.org/10.1785/0120180137
- 929 Fossen, H., Johansen, T. E. S., Hesthammer, J., & Rotevatn, A. (2005). Fault interaction in porous
- 930 sandstone and implications for reservoir management; examples from southern Utah. AAPG
- 931 Bulletin, 89(12). Retrieved from https://pubs.geoscienceworld.org/aapg/aapgbull/article-
- abstract/89/12/1593/132681/Fault-interaction-in-porous-sandstone-and
- 933 Fossen, Haakon, & Rotevatn, A. (2016). Fault linkage and relay structures in extensional
- 934 settings—A review. Earth-Science Reviews, 154, 14–28.
- 935 https://doi.org/10.1016/j.earscirev.2015.11.014
- Friedrich, A. M., Wernicke, B. P., Niemi, N. A., Bennett, R. A., & Davis, J. L. (2003). Comparison of
- 937 geodetic and geologic data from the Wasatch region, Utah, and implications for the spectral
- character of Earth deformation at periods of 10 to 10 million years. Journal of Geophysical
- 939 Research: Solid Earth, 108(B4). https://doi.org/10.1029/2001JB000682
- 940 Galli, P. (2020). Recurrence times of central-southern Apennine faults (Italy): Hints from
- 941 palaeoseismology. Terra Nova, 32(6), 399–407. https://doi.org/10.1111/ter.12470
- 942 Gartrell, A., Torres, J., Dixon, M., Keep, M., Gartrell, A., Torres, J., et al. (2016). Mesozoic rift
- onset and its impact on the sequence stratigraphic architecture of the Northern Carnarvon
- 944 Basin. The APPEA Journal, 56(1), 143–158. https://doi.org/10.1071/AJ15012
- 945 Gartrell, A. P. (2000). Rheological controls on extensional styles and the structural evolution of
- 946 the Northern Carnaryon Basin, North West Shelf, Australia. Australian Journal of Earth Sciences,
- 947 47(2), 231–244. https://doi.org/10.1046/j.1440-0952.2000.00776.x
- 948 Gauriau, J., & Dolan, J. F. (2021). Relative Structural Complexity of Plate-Boundary Fault
- 949 Systems Controls Incremental Slip-Rate Behavior of Major Strike-Slip Faults. Geochemistry,
- 950 Geophysics, Geosystems, 22(11), e2021GC009938. https://doi.org/10.1029/2021GC009938
- 951 Gómez-Novell, O., García-Mayordomo, J., Ortuño, M., Masana, E., & Chartier, T. (2020). Fault
- 952 System-Based Probabilistic Seismic Hazard Assessment of a Moderate Seismicity Region: The
- 953 Eastern Betics Shear Zone (SE Spain). Frontiers in Earth Science, 8.
- 954 https://doi.org/10.3389/feart.2020.579398

- Goodall, H. J., Gregory, L. C., Wedmore, L. N. J., McCaffrey, K. J. W., Amey, R. M. J., Roberts, G.
- 956 P., et al. (2021). Determining Histories of Slip on Normal Faults With Bedrock Scarps Using
- 957 Cosmogenic Nuclide Exposure Data. Tectonics, 40(3), e2020TC006457.
- 958 https://doi.org/10.1029/2020TC006457
- 959 Gupta, A., & Scholz, C. H. (2000). A model of normal fault interaction based on observations and
- 960 theory. Journal of Structural Geology, 22(7), 865–879. https://doi.org/10.1016/S0191-
- 961 8141(00)00011-0
- Harris, R. A., & Simpson, R. W. (1998). Suppression of large earthquakes by stress shadows: A
- comparison of Coulomb and rate-and-state failure. Journal of Geophysical Research, 103(B10),
- 964 24439. https://doi.org/10.1029/98JB00793
- Herrero-Barbero, P., Álvarez-Gómez, J. A., Tsige, M., & Martínez-Díaz, J. J. (2023). Deterministic
- seismic hazard analysis from physics-based earthquake simulations in the Eastern Betics (SE
- 967 Iberia). Engineering Geology, 327, 107364. https://doi.org/10.1016/j.enggeo.2023.107364
- Holden, N., Alaei, B., Skurtveit, E., & Braathen, A. (2024). Implications of depth conversion on
- 969 fault geometries and fault-risk assessment in the Smeaheia CO2 storage site, northern North
- 970 Sea. Geoenergy, 0(ja), geoenergy2024-006. https://doi.org/10.1144/geoenergy2024-006
- 971 lezzi, F., Roberts, G. P., & Faure Walker, J. (2020). Throw-rate variations within linkage zones
- during the growth of normal faults: Case studies from the Western Volcanic Zone, Iceland.
- 973 Journal of Structural Geology, 133, 103976. https://doi.org/10.1016/j.jsg.2020.103976
- 974 lezzi, F., Roberts, G., Faure Walker, J., Papanikolaou, I., Ganas, A., Deligiannakis, G., et al. (2021).
- 975 Temporal and spatial earthquake clustering revealed through comparison of millennial strain-
- rates from 36Cl cosmogenic exposure dating and decadal GPS strain-rate. Scientific Reports,
- 977 11(1), 23320. https://doi.org/10.1038/s41598-021-02131-3
- Jackson, C. A.-L., Bell, R. E., Rotevatn, A., & Tvedt, A. B. M. (2017). Techniques to determine the
- kinematics of synsedimentary normal faults and implications for fault growth models.
- 980 Geological Society, London, Special Publications, 439(1), 187–217.
- 981 https://doi.org/10.1144/SP439.22
- 982 Karner, G. D., & Driscoll, N. W. (1999). Style, timing and distribution of tectonic deformation
- 983 across the Exmouth Plateau, northwest Australia, determined from stratal architecture and
- 984 quantitative basin modelling. In C. MacNiocall & P. Ryan (Eds.), Continental Tectonics (Vol. 164,
- pp. 271–311). London, UK: Geological Society of London.
- 986 https://doi.org/10.2973/odp.proc.sr.122.1992

- 987 Kattenhorn, S. A., Aydin, A., & Pollard, D. D. (2000). Joints at high angles to normal fault strike:
- an explanation using 3-D numerical models of fault-perturbed stress fields. Journal of Structural
- 989 Geology, 22(1), 1–23. https://doi.org/10.1016/S0191-8141(99)00130-3
- 990 Lathrop, B. A., Jackson, C. A.-L., Bell, R. E., & Rotevatn, A. (2021). Normal Fault Kinematics and
- the Role of Lateral Tip Retreat: An Example From Offshore NW Australia. Tectonics, 40(5),
- 992 e2020TC006631. https://doi.org/10.1029/2020TC006631
- Lathrop, B. A., Jackson, C. a.-L., Bell, R. E., & Rotevatn, A. (2022). Displacement/Length Scaling
- 994 Relationships for Normal Faults; a Review, Critique, and Revised Compilation. Frontiers in Earth
- 995 Science, 10. https://doi.org/10.3389/feart.2022.907543
- 296 Lin, J., & Stein, R. S. (2004). Stress triggering in thrust and subduction earthquakes and stress
- 997 interaction between the southern San Andreas and nearby thrust and strike-slip faults. Journal
- of Geophysical Research, 109(B2). https://doi.org/10.1029/2003JB002607
- 999 Magee, C., & Jackson, C. A.-L. (2020a). Can we relate the surface expression of dike-induced
- normal faults to subsurface dike geometry? Geology, 49(4), 366–371.
- 1001 https://doi.org/10.1130/G48171.1
- 1002 Magee, C., & Jackson, C. A.-L. (2020b). Seismic reflection data reveal the 3D structure of the
- newly discovered Exmouth Dyke Swarm, offshore NW Australia. Solid Earth, 11(2), 579–606.
- 1004 https://doi.org/10.5194/se-11-579-2020
- 1005 Magee, C., Love, V., Fayez, K., Andrews, B., Rivas-Dorado, S., Jackson, C., et al. (2023).
- 1006 Quantifying Dyke-Induced Graben and Dyke Structure Using 3D Seismic Reflection Data and The
- 1007 Role of Interpretation Bias. Тектопіка, 1(2), 32–53.
- 1008 https://doi.org/10.55575/tektonika2023.1.2.25
- 1009 Manighetti, I., King, G., & Sammis, C. G. (2004). The role of off-fault damage in the evolution of
- normal faults. Earth and Planetary Science Letters, 217.
- 1011 Mansfield, C., & Cartwright, J. (2001). Fault growth by linkage: observations and implications
- from analogue models. Journal of Structural Geology, 23(5), 745–763.
- 1013 https://doi.org/10.1016/S0191-8141(00)00134-6
- 1014 Mäntyniemi, P., Tatevossian, R. E., & Tatevossian, T. N. (2014). Uncertain historical earthquakes
- and seismic hazard: theoretical and practical considerations. Geomatics, Natural Hazards and
- 1016 Risk, 5(1), 1–6. https://doi.org/10.1080/19475705.2012.751633

- 1017 Manzocchi, T., Walsh, J. J., & Nicol, A. (2006). Displacement accumulation from earthquakes on
- isolated normal faults. Journal of Structural Geology, 28(9), 1685–1693.
- 1019 https://doi.org/10.1016/j.jsg.2006.06.006
- Martinez, C., Chiarella, D., Jackson, C. A.-L., Rennie, H., & Scarselli, N. (2024). Syn-rift tectono-
- stratigraphic development of the Thebe-0 fault system, Exmouth Plateau, offshore NW
- 1022 Australia: The role of fault-scarp degradation. Basin Research, 36(1), e12842.
- 1023 https://doi.org/10.1111/bre.12842
- 1024 McClymont, A. F., Villamor, P., & Green, A. G. (2009). Fault displacement accumulation and slip
- rate variability within the Taupo Rift (New Zealand) based on trench and 3-D ground-
- penetrating radar data. Tectonics, 28(4). https://doi.org/10.1029/2008TC002334
- 1027 Mechernich, S., Schneiderwind, S., Mason, J., Papanikolaou, I. D., Deligiannakis, G., Pallikarakis,
- 1028 A., et al. (2018). The Seismic History of the Pisia Fault (Eastern Corinth Rift, Greece) From Fault
- 1029 Plane Weathering Features and Cosmogenic 36Cl Dating. Journal of Geophysical Research: Solid
- 1030 Earth, 123(5), 4266–4284. https://doi.org/10.1029/2017JB014600
- 1031 Meyer, V., Nicol, A., Childs, C., Walsh, J. J., & Watterson, J. (2002). Progressive localisation of
- strain during the evolution of a normal fault population. Journal of Structural Geology, 24(8),
- 1033 1215–1231. https://doi.org/10.1016/S0191-8141(01)00104-3
- 1034 Mia, M. S., Abdelmeguid, M., Harris, R. A., & Elbanna, A. E. (2024). Rupture Jumping and Seismic
- 1035 Complexity in Models of Earthquake Cycles for Fault Stepovers with Off-Fault Plasticity. Bulletin
- of the Seismological Society of America, 114(3), 1466–1480.
- 1037 https://doi.org/10.1785/0120230249
- 1038 Mignan, A., Danciu, L., & Giardini, D. (2015). Reassessment of the Maximum Fault Rupture
- Length of Strike-Slip Earthquakes and Inference on Mmax in the Anatolian Peninsula, Turkey.
- Seismological Research Letters, 86(3). Retrieved from
- https://pubs.geoscienceworld.org/ssa/srl/article-abstract/86/3/890/315715/Reassessment-of-
- 1042 the-Maximum-Fault-Rupture-Length
- Mildon, Z. K., Roberts, G. P., Faure Walker, J. P., Beck, J., Papanikolaou, I., Michetti, A. M., et al.
- 1044 (2022). Surface faulting earthquake clustering controlled by fault and shear-zone interactions.
- 1045 Nature Communications, 13(1), 7126. https://doi.org/10.1038/s41467-022-34821-5
- 1046 Milner, K., Page, M. T., Field, E. H., Parsons, T., Biasi, G. P., & Shaw, B. E. (2013). Defining the
- inversion rupture set via plausibility filters (USGS Open-File Report No. 1165).

- Nicol, A., Watterson, J., Walsh, J. J., & Childs, C. (1996). The shapes, major axis orientations and
- displacement patterns of fault surfaces. Journal of Structural Geology, 18(2), 235–248.
- 1050 https://doi.org/10.1016/S0191-8141(96)80047-2
- Nicol, A., Walsh, J. J., Watterson, J., & Underhill, J. R. (1997). Displacement rates of normal
- 1052 faults. Nature, 390, 157–159. https://doi.org/10.1038/36548
- Nicol, A., Walsh, J. J., Villamor, P., Seebeck, H., & Berryman, K. R. (2010). Normal fault
- interactions, paleoearthquakes and growth in an active rift. Journal of Structural Geology, 32(8),
- 1055 1101–1113. https://doi.org/10.1016/j.jsg.2010.06.018
- Nicol, A, Robinson, R., Van Dissen, R., & Harvison, A. (2016). Variability of recurrence interval
- and single-event slip for surface-rupturing earthquakes in New Zealand. New Zealand Journal of
- 1058 Geology and Geophysics, 59(1), 97–116. https://doi.org/10.1080/00288306.2015.1127822
- Nicol, Andrew, Walsh, J., Berryman, K., & Nodder, S. (2005). Growth of a normal fault by the
- accumulation of slip over millions of years. Journal of Structural Geology, 27(2), 327–342.
- 1061 https://doi.org/10.1016/j.jsg.2004.09.002
- Nixon, C. W., Bull, J. M., & Sanderson, D. J. (2014). Localized vs distributed deformation
- associated with the linkage history of an active normal fault, Whakatane Graben, New Zealand.
- Journal of Structural Geology, 69, 266–280. https://doi.org/10.1016/j.jsg.2014.06.005
- Nixon, C. W., McNeill, L. C., Gawthorpe, R. L., Shillington, D. J., Michas, G., Bell, R. E., et al.
- 1066 (2024). Increasing fault slip rates within the Corinth Rift, Greece: A rapidly localising active rift
- fault network. Earth and Planetary Science Letters, 636, 118716.
- 1068 https://doi.org/10.1016/j.epsl.2024.118716
- 1069 Onderdonk, N. W., McGill, S. F., & Rockwell, T. K. (2015). Short-term variations in slip rate and
- size of prehistoric earthquakes during the past 2000 years on the northern San Jacinto fault
- zone, a major plate-boundary structure in southern California. Lithosphere, 7(3), 211–234.
- 1072 https://doi.org/10.1130/L393.1
- Pace, B., Bocchini, G. M., & Boncio, P. (2014). Do static stress changes of a moderate-magnitude
- earthquake significantly modify the regional seismic hazard? Hints from the L'Aquila 2009
- normal-faulting earthquake (Mw 6.3, central Italy). Terra Nova, 26(6), 430–439.
- 1076 https://doi.org/10.1111/ter.12117
- Pace, B., Visini, F., & Peruzza, L. (2016a). FiSH: MATLAB Tools to Turn Fault Data into Seismic-
- Hazard Models. Seismological Research Letters, 87(JANUARY), 1–13.
- 1079 https://doi.org/10.1785/0220150189

- Pace, B., Visini, F., & Peruzza, L. (2016b). FiSH: MATLAB Tools to Turn Fault Data into Seismic-
- Hazard Models. Seismological Research Letters, 87(2A), 374–386.
- 1082 https://doi.org/10.1785/0220150189
- Pan, S., Bell, R. E., Jackson, C. A.-L., & Naliboff, J. (2022). Evolution of normal fault displacement
- and length as continental lithosphere stretches. Basin Research, 34(1), 121–140.
- 1085 https://doi.org/10.1111/bre.12613
- 1086 Peacock, D. C. P., Nixon, C. W., Rotevatn, A., Sanderson, D. J., & Zuluaga, L. F. (2017). Interacting
- faults. Journal of Structural Geology, 97, 1–22. https://doi.org/10.1016/j.jsg.2017.02.008
- 1088 Pesci, A., Teza, G., & Casula, G. (2009). Improving strain rate estimation from velocity data of
- non-permanent GPS stations: the Central Apennine study case (Italy). GPS Solutions, 13(4),
- 1090 249–261. https://doi.org/10.1007/s10291-009-0118-3
- Reeve, M. T., Jackson, C. A.-L., Bell, R. E., Magee, C., & Bastow, I. D. (2016). The stratigraphic
- record of prebreakup geodynamics: Evidence from the Barrow Delta, offshore Northwest
- 1093 Australia. Tectonics, 35(8), 1935–1968. https://doi.org/10.1002/2016TC004172
- Reeve, M. T., Magee, C., Jackson, C. a.-L., Bell, R., & Bastow, I. D. (2022). Stratigraphic record of
- continental breakup, offshore NW Australia. Basin Research, 34(3), 1220–1243.
- 1096 https://doi.org/10.1111/bre.12656
- 1097 Roberts, G. P. (2007). Fault orientation variations along the strike of active normal fault systems
- in Italy and Greece: Implications for predicting the orientations of subseismic-resolution faults
- in hydrocarbon reservoirs. AAPG Bulletin, 91(1), 1–20. https://doi.org/10.1306/08300605146
- Roberts, G. P., Sgambato, C., Mildon, Z. K., Iezzi, F., Beck, J., Robertson, J., et al. (2024). Spatial
- migration of temporal earthquake clusters driven by the transfer of differential stress between
- neighbouring fault/shear-zone structures. Journal of Structural Geology, 181, 105096.
- 1103 https://doi.org/10.1016/j.jsg.2024.105096
- Roberts, G. P., F, I., C, S., J, R., J, B., Z.k, M., et al. (2025). Characteristics and modelling of slip-
- 1105 rate variability and temporal earthquake clustering across a distributed network of active
- normal faults constrained by in situ 36Cl cosmogenic dating of fault scarp exhumation, central
- 1107 Italy. Journal of Structural Geology, 195, 105391. https://doi.org/10.1016/j.jsg.2025.105391
- 1108 Roberts, Gerald P, & Michetti, A. M. (2004). Spatial and temporal variations in growth rates
- along active normal fault systems: an example from The Lazio–Abruzzo Apennines, central Italy.
- Journal of Structural Geology, 26(2), 339–376. https://doi.org/10.1016/S0191-8141(03)00103-2

- Roche, V., Homberg, C., & Rocher, M. (2013). Fault nucleation, restriction, and aspect ratio in
- layered sections: Quantification of the strength and stiffness roles using numerical modeling.
- Journal of Geophysical Research: Solid Earth, 118(8), 4446–4460.
- 1114 https://doi.org/10.1002/jgrb.50279
- Rodriguez Piceda, C., Mildon, Z. K., van den Ende, M., Ampuero, J.-P., & Andrews, B. J. (2025).
- Normal Fault Interactions in Seismic Cycles and the Impact of Fault Network Geometry. Journal
- of Geophysical Research: Solid Earth, 130(4), e2024JB030382.
- 1118 https://doi.org/10.1029/2024JB030382
- Romanet, P., Bhat, H. S., Jolivet, R., & Madariaga, R. (2018). Fast and Slow Slip Events Emerge
- Due to Fault Geometrical Complexity. Geophysical Research Letters, 45(10), 4809–4819.
- 1121 https://doi.org/10.1029/2018GL077579
- Rotevatn, A., Jackson, C. A.-L., Tvedt, A. B. M., Bell, R. E., & Blækkan, I. (2019). How do normal
- faults grow? Journal of Structural Geology, (August), 0–1.
- 1124 https://doi.org/10.1016/j.jsg.2018.08.005
- 1125 Schaaf, A., & Bond, C. E. (2019). Quantification of uncertainty in 3-D seismic interpretation:
- implications for deterministic and stochastic geomodeling and machine learning. Solid Earth,
- 1127 10(4), 1049–1061. https://doi.org/10.5194/se-10-1049-2019
- 1128 Schlagenhauf, A., Manighetti, I., Malavieille, J., & Dominguez, S. (2008). Incremental growth of
- normal faults: Insights from a laser-equipped analog experiment. Earth and Planetary Science
- 1130 Letters, 273(3), 299–311. https://doi.org/10.1016/j.epsl.2008.06.042
- 1131 Scholz, C. H., & Contreras, J. C. (1998). Mechanics of continental rift architecture. Geology,
- 1132 26(11), 967–970.
- 1133 Schwartz, D. P., & Coppersmith, K. J. (1984). Fault behavior and characteristic earthquakes:
- examples from the Wasatch and San Andreas fault zones (USA). J. Geophys. Res., 89(B7), 5681–
- 1135 5698. https://doi.org/10.1029/JB089iB07p05681
- Scotti, O., Visini, F., Faure Walker, J., Peruzza, L., Pace, B., Benedetti, L., et al. (2021). Which
- Fault Threatens Me Most? Bridging the Gap Between Geologic Data-Providers and Seismic Risk
- Practitioners. Frontiers in Earth Science, 8. https://doi.org/10.3389/feart.2020.626401
- 1139 Sgambato, C., Faure Walker, J. P., & Roberts, G. P. (2020). Uncertainty in strain-rate from field
- measurements of the geometry, rates and kinematics of active normal faults: Implications for
- seismic hazard assessment. Journal of Structural Geology, 131, 103934.
- 1142 https://doi.org/10.1016/j.jsg.2019.103934

- 1143 Sgambato, C., Faure Walker, J. P., Roberts, G. P., Mildon, Z. K., & Meschis, M. (2023). Influence
- of Fault System Geometry and Slip Rates on the Relative Role of Coseismic and Interseismic
- 1145 Stresses on Earthquake Triggering and Recurrence Variability. Journal of Geophysical Research:
- Solid Earth, 128(11), e2023JB026496. https://doi.org/10.1029/2023JB026496
- 1147 Sgambato, C., Roberts, G. P., Iezzi, F., Faure Walker, J. P., Beck, J., Mildon, Z. K., et al. (2025).
- 1148 Millennial Slip-Rates Variability of Along-Strike Active Faults in the Italian Southern Apennines
- Revealed by Cosmogenic 36Cl Dating of Fault Scarps. Tectonics, 44(3), e2024TC008529.
- 1150 https://doi.org/10.1029/2024TC008529
- 1151 Shaw, B. E., Milner, K., Field, E. H., Richards-Dinger, K., Gilchrist, J. J., Dieterich, J. H., & Jordan,
- T. H. (2018). A physics-based earthquake simulator replicates seismic hazard statistics across
- 1153 California. Science Advances, 4(8). https://doi.org/10.1126/sciadv.aau0688
- 1154 Soliva, R., Benedicto, A., & Maerten, L. (2006). Spacing and linkage of confined normal faults:
- 1155 Importance of mechanical thickness. Journal of Geophysical Research: Solid Earth, 111(1), 1–17.
- 1156 https://doi.org/10.1029/2004JB003507
- 1157 Stein, R. S. (1999). The role of stress transfer in earthquake occurrence. Nature, 402(6762),
- 1158 605–609. https://doi.org/10.1038/45144
- 1159 Swafford, L., & Stein, S. (2007). Limitations of the short earthquake record for seismicity and
- seismic hazard studies. In S. Stein & S. Mazzotti (Eds.), Continental Intraplate Earthquakes:
- Science, Hazard, and Policy Issues (p. 0). Geological Society of America.
- 1162 https://doi.org/10.1130/2007.2425(04)
- 1163 Sylvester, A. G. (1988). Strike-slip faults. GSA Bulletin, 100(11), 1666–1703.
- https://doi.org/10.1130/0016-7606(1988)100%253C1666:SSF%253E2.3.CO;2
- 1165 Taylor, S. K., Nicol, A., & Walsh, J. J. (2008). Displacement loss on growth faults due to sediment
- 1166 compaction. Journal of Structural Geology, 30(3), 394–405.
- 1167 https://doi.org/10.1016/j.jsg.2007.11.006
- Toda, S., & Enescu, B. (2011). Rate/state Coulomb stress transfer model for the CSEP Japan
- seismicity forecast. Earth, Planets and Space, 63(3), 171–185.
- 1170 https://doi.org/10.5047/eps.2011.01.004
- Toda, S., & Stein, R. S. (2018). Why Aftershock Duration Matters for Probabilistic Seismic Hazard
- 1172 Assessment. Bull. Seismol. Soc. Am., 108(3), 1414–1426. https://doi.org/10.1785/0120170270

- 1173 Toda, S., Stein, R. S., Reasenberg, P. A., Dieterich, J. H., & Yoshida, A. (1998). Stress transferred
- by the 1995 Mw = 6.9 Kobe, Japan, shock: Effect on aftershocks and future earthquake
- probabilities. Journal of Geophysical Research: Solid Earth, 103(B10), 24543–24565.
- 1176 https://doi.org/10.1029/98JB00765
- 1177 Torabi, A., & Berg, S. S. (2011). Scaling of fault attributes: A review. Marine and Petroleum
- Geology, 28(8), 1444–1460. https://doi.org/10.1016/j.marpetgeo.2011.04.003
- 1179 Valentini, A., Visini, F., & Pace, B. (2017). Integrating faults and past earthquakes into a
- probabilistic seismic hazard model for peninsular Italy. Natural Hazards and Earth System
- 1181 Sciences, 17(11), 2017–2039. https://doi.org/10.5194/nhess-17-2017-2017
- 1182 Verdecchia, A., Carena, S., Pace, B., & DuRoss, C. B. (2019). The effect of stress changes on time-
- dependent earthquake probabilities for the central Wasatch fault zone, Utah, USA. Geophysical
- Journal International, 219(2), 1065–1081. https://doi.org/10.1093/gji/ggz336
- Walsh, J. J., Childs, C., Imber, J., Manzocchi, T., Watterson, J., & Nell, P. A. R. (2003). Strain
- localisation and population changes during fault system growth within the Inner Moray Firth,
- Northern North Sea. Journal of Structural Geology, 25(2), 307–315.
- 1188 https://doi.org/10.1016/S0191-8141(02)00028-7
- 1189 Wechsler, N., Rockwell, T. K., & Klinger, Y. (2018). Variable slip-rate and slip-per-event on a
- plate boundary fault: The Dead Sea fault in northern Israel. Tectonophysics, 722, 210–226.
- 1191 https://doi.org/10.1016/j.tecto.2017.10.017
- 1192 Weldon, R., Scharer, K., Fumal, T., & Biasi, G. (2004). Wrightwood and the earthquake cycle:
- 1193 What a long recurrence record tells us about how faults work. GSA Today, 14(9), 4–10.
- https://doi.org/10.1130/1052-5173(2004)014%253C4:WATECW%253E2.0.CO;2
- 1195 Williams, J. N., Werner, M. J., Goda, K., Wedmore, L. N., De Risi, R., Biggs, J., et al. (2023). Fault-
- based probabilistic seismic hazard analysis in regions with low strain rates and a thick
- seismogenic layer: a case study from Malawi. Geophysical Journal International, 233(3), 2172–
- 1198 2207. https://doi.org/10.1093/gji/ggad060
- 1199 Woodcock, N. (1986). The role of strike-slip fault systems at plate boundaries. Philosophical
- 1200 Transactions of the Royal Society of London. Series A, Mathematical and Physical Sciences,
- 317(1539). Retrieved from https://royalsocietypublishing.org/doi/abs/10.1098/rsta.1986.0021
- 1202 Yin, Y., Galvez, P., Heimisson, E. R., & Wiemer, S. (2023). The role of three-dimensional fault
- interactions in creating complex seismic sequences. Earth and Planetary Science Letters, 606,
- 1204 118056. https://doi.org/10.1016/j.epsl.2023.118056

- 1205 Youngs, R. R., & Coppersmith, K. J. (1985). Implications of fault slip rates and earthquake
- recurrence models to probabilistic seismic hazard estimates. Bulletin of the Seismological
- 1207 Society of America, 75(4), 939–964. https://doi.org/10.1785/BSSA0750040939
- 1208 Zinke, R., Dolan, J. F., Rhodes, E. J., Van Dissen, R., McGuire, C. P., Hatem, A. E., et al. (2019).
- Multimillennial Incremental Slip Rate Variability of the Clarence Fault at the Tophouse Road
- 1210 Site, Marlborough Fault System, New Zealand. Geophysical Research Letters, 46(2), 717–725.
- 1211 https://doi.org/10.1029/2018GL080688
- 1212 Key supplementary information

1214

1215

12161217

12181219

1220

1221

1222

1223

12241225

1226

Supplementary 1: Time-depth conversion

The conversion of measured depth values, which are in two-way-time (TWT) to depth in metres, is a considerable source of error in the quantitative throw analysis of faults imaged in seismic data (Holden et al., 2024). This arises because seismic velocities are obtained from borehole data, which effectively provide a 1D snapshot of the subsurface and do not capture spatial variabilities. Additionally, similar to elsewhere in the Exmouth Plateau, wells were drilled in the footwall of normal faults, limiting the depth range and not capturing any potential differences between footwall and hanging wall seismic velocities. The four wells in the study area have checkshot data for depth ranges of 1200 m and 3166 m, with limited variations between each well (Table S1). We convert from time to depth by calculating a polynomial line of best fit to the combined checkshot data (Fig S1). Considering the differences between wells, and the limitations of using check-shot data, we acknowledge a ±10% variation in seismic velocity may occur across the study area.

Table S1.1: Checkshot data from Chandon-1, Chandon-2, Chandon-3, and Yellowglen

Chan	Chandon-1		Chandon-2		don-3	Yellowglen	
One way	Measured	One way	Measured	One way	Measured	One way	Measured
time (s)	depth (m)	time (s)	depth (m)	time (s)	depth (m)	time (s)	depth (m)
0	28.9	0.000	0022.0	0.000	0022.3	0.000	0022.0
0.797	1225	0.786	1200.3	0.806	1229.6	0.813	1238.0
0.929	1459.7	0.806	1230.5	0.826	1259.9	0.834	1269.1
0.990	1596	0.825	1260.8	0.846	1290.1	0.852	1299.4
1.018	1648.5	0.843	1291.0	0.865	1320.3	0.871	1328.7
1.046	1720	0.861	1321.4	0.883	1350.6	0.889	1358.9
1.173	1929.8	0.879	1351.6	0.901	1380.8	0.906	1389.1
1.220	2053.0	0.896	1381.8	0.919	1411.0	0.923	1419.4

1.255	2143.0	0.912	1412.1	0.936	1441.4	0.940	1449.6
1.362	2348.0	0.928	1442.6	0.952	1471.6	0.956	1479.9
1.371	2405.0	0.943	1472.9	0.968	1501.8	0.972	1510.1
1.403	2475.0	0.958	1503.1	0.983	1532.0	0.989	1540.3
1.434	2548.0	0.973	1533.4	0.998	1562.3	1.006	1570.6
1.476	2642.0	0.988	1563.4	1.013	1592.5	1.022	1600.8
1.489	2680.2	1.003	1593.6	1.028	1622.8	1.037	1631.1
1.507	2714.8	1.017	1623.9	1.043	1653.0	1.053	1661.4
1.513	2748.9	1.031	1654.1	1.058	1683.1	1.068	1691.5
1.587	2943.8	1.045	1684.3	1.073	1713.4	1.082	1721.8
1.606	3022.8	1.059	1714.6	1.088	1743.5	1.097	1752.0
		1.075	1744.8	1.104	1773.7	1.112	1782.3
		1.091	1775.0	1.120	1804.0	1.127	1812.5
		1.106	1805.1	1.135	1834.3	1.142	1842.8
		1.120	1835.4	1.151	1864.7	1.155	1873.0
		1.134	1865.6	1.166	1894.9	1.169	1903.3
		1.148	1895.8	1.180	1925.1	1.182	1933.6
		1.161	1926.0	1.192	1955.4	1.198	1963.8
		1.174	1956.2	1.204	1985.7	1.213	1993.9
		1.187	1986.4	1.215	2015.9	1.228	2024.1
		1.199	2016.7	1.227	2046.1	1.243	2054.5
		1.210	2047.2	1.238	2076.3	1.257	2084.7
		1.222	2077.5	1.249	2106.6	1.272	2114.9
		1.234	2107.7	1.261	2136.8	1.286	2145.2
		1.248	2138.0	1.275	2167.1	1.299	2175.4
		1.262	2168.1	1.288	2197.3	1.311	2205.6
		1.275	2198.4	1.301	2227.6	1.323	2236.0
		1.289	2228.6	1.314	2257.8	1.335	2266.2
		1.302	2258.9	1.327	2288.1	1.349	2296.3
		1.316	2289.0	1.341	2318.3	1.364	2326.5
		1.329	2319.3	1.355	2348.5	1.378	2356.8
		1.341	2349.5	1.369	2378.7	1.392	2387.0
		1.353	2379.7	1.383	2409.0	1.405	2417.3
		1.365	2410.0	1.396	2439.3	1.417	2447.6

			1		,
1.378	2440.3	1.410	2469.5	1.429	2477.8
1.392	2470.5	1.423	2499.7	1.442	2508.0
1.405	2500.7	1.436	2530.0	1.454	2538.3
1.418	2531.1	1.449	2560.2	1.466	2568.5
1.431	2561.3	1.462	2590.4	1.478	2598.7
1.444	2591.5	1.475	2620.7	1.490	2628.9
1.456	2621.8	1.488	2651.0	1.501	2659.2
1.469	2651.9	1.500	2681.2	1.512	2689.5
1.481	2682.1	1.513	2711.4	1.523	2719.7
1.491	2712.4	1.524	2741.6	1.534	2749.9
1.501	2742.6	1.534	2771.9		
1.511	2772.9	1.544	2802.2		
1.520	2803.2	1.555	2832.4		
1.531	2833.4	1.563	2862.6		
1.542	2863.7	1.574	2892.8		
1.553	2893.9	1.585	2923.1		
1.563	2924.1	1.595	2953.3		
1.573	2954.3	1.605	2983.5		
1.583	2984.6	1.614	3013.8		
1.593	3014.8	1.624	3044.0		
1.602	3045.1	1.634	3074.3		
1.612	3075.3	1.643	3104.5		
1.622	3105.5	1.653	3134.8		
		1.662	3165.0		

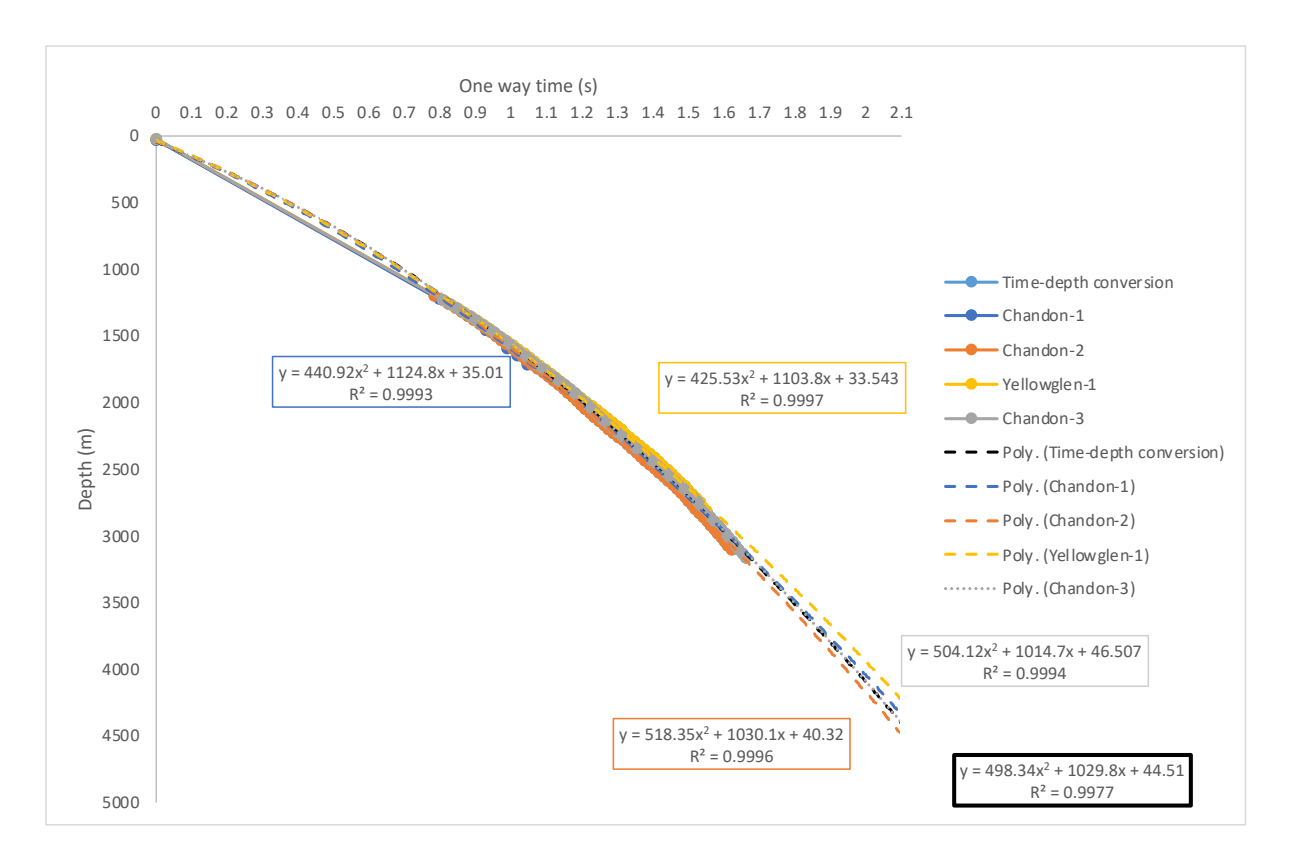


Figure S1.1: Extrapolated time-depth relationships for the boreholes used to depth-covert measurements made in time (s).

1228

1230 Supplementary 2: Throw extraction and slip-rate, errors and methods.

- 1231 Fault cut off data, extracted for each mapped horizon-fault intersection, can be used to
- calculate a range of fault parameters including throw, heave, and displacement (aka slip)
- 1233 (Figure S2.1). Cut-off data can either be sampled at the horizon-fault intersection (i.e.,
- discontinuous cut-off, triangle), or the regional horizon dip can be projected onto the fault
- surface to capture non-discrete strain (i.e., continuous cut-offs, diamond). In our study, we
- utilise the latter to capture the long-term patterns in slip associated with the time intervals of
- interest.
- 1238 Fault parameters derived from continuous cut-offs are prone to a greater degree of uncertainty
- when compared to discontinuous cut offs (Andrews et al., 2024). To account for this, we apply
- errors to the throw, dip, and horizon ages (Table S2.1) and propagate these errors through the
- 1241 calculation of slip-rate. To achieve this, we first calculate a minimum and maximum Δthrow:

1242
$$\Delta \text{throw}_{\min} = \text{Throw}_{h2_{\min}} - \text{Throw}_{h1_{\max}}$$
 (Equation S2.1)

1243
$$\Delta \text{throw}_{\text{max}} = \text{Throw}_{\text{h2}_{\text{max}}} - \text{Throw}_{\text{h1}_{\text{min}}}$$
 (Equation S2.2)

We then calculate the maximum and minimum displacement, or slip:

$$Slip_{min} = \frac{\Delta throw_{min}}{\cos(Dip_{max})}$$
 (Equation S2.3)

$$1246 Slip_{max} = \frac{\Delta throw_{max}}{\cos (Dip_{min})} (Equation S2.4)$$

1247 Minimum and maximum slip-rate (SR) values are then calculated:

$$SR_{min} = \frac{Slip_{min}*1000}{(Age_{H2}-250000)-(Age_{H1}+250000)}$$
 (Equation S2.5)

$$1249 SR_{max} = \frac{Slip_{max}*1000}{(Age_{H2}+250000)-(Age_{H1}-250000)} (Equation S2.6)$$

- 1250 Errors are presented as error bars showing the minimum and maximum slip rate. It should also
- be noted that there are times where it was not possible to use the same horizon across the full
- fault, in this case, the next oldest horizons were used when calculating slip-rate. This could
- cause different slip rate intervals at different locations along the fault. A summary of intervals
- used for each fault is shown in Figure S2.2, as well as provided in the metadata of the slip-rate
- supplementary information (Supplementary 3).

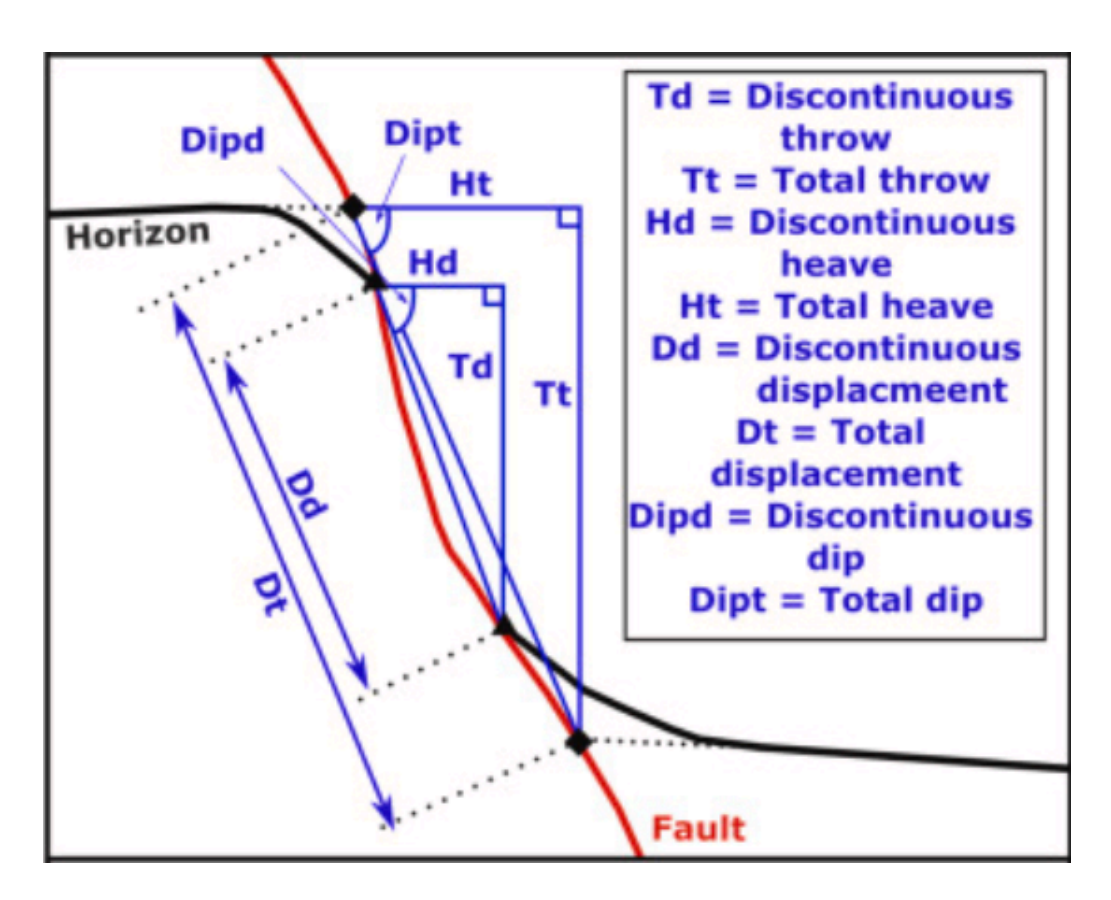


Figure S2.1: Potential measurements using fault cut-offs.

Table S2.1: Error calculations used in the calculation of slip-rate. *error % based on findings of Andrews et al., 2024.

Measurement	Error
Throw*	$\pm 8\%$ or the limit of visibility, whichever is larger.
Dip*	±15%
Horizon age	±250 kyr

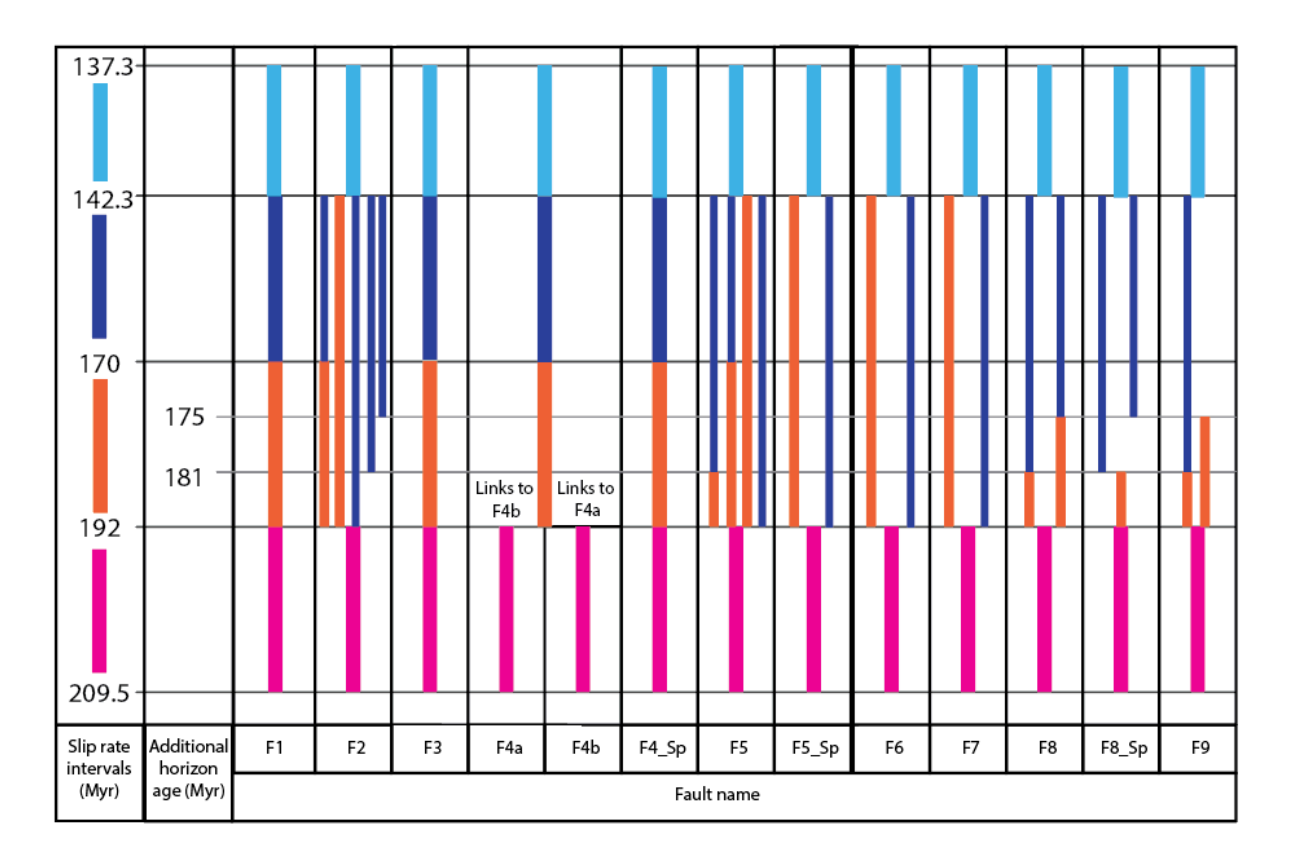


Figure S2.2: Age framework used to calculate slip-rate, showing where different intervals were required for some faults due to e.g., the 170 Myr horizon not being present along part, or all, of a faults length.

Supplementary 4: FiSH modelling inputs and supplementary results

Table S4.1: Input parameters for FiSH modelling. Length data was extracted directly from QGIS, accounting for changes in fault strike, and was used to calculate the seismogenic thickness of the fault. Average values were calculated for Dip and slip-rate for each time period. For all faults, we use the Wells and Coppersmith 1994 length to magnitude relationship for normal faults, and NaN values for Mobs, sdMobs and last earthquake time.

			Seis.	RA:	T1:	T2:	T3:	T4:	T4v2:
Fault	Length	Dip ()	thickness	SR _{209.5} -	SR _{209.5} -	SR ₁₉₂ -	SR ₁₇₀₋	SR _{142.3} -	SR _{142.3} -
name	(km)	Βίρ ()	(km)	137.3Ma	192Ma	170Ma	142.3Ma	137.3Ma	137.3Ma
		4.4	. ,	(mm/yr)	(mm/yr)	(mm/yr)	(mm/yr)	(mm/yr)	(mm/yr)
F1		44 (RA, T1,							
(Single	17.7	T2) 43 _{(T3, T4,}	5.7	0.0032	0.0025	0.0028	0.0013	0.0197	0.0197
fault)		T4v2)							
F2	7.4	45	2.4	0.0022	0.0007	0.0003	0.0053	0.0136	0.0136
F3	3.3	40	1.0	0.0017	0.0009	0.0007	0.0005	0.0182	0.0182
F4*	8.3	44	2.7	0.0035	n/a	0.0020	0.0043	0.0222	0.0222
F4a*	2.9	41	0.9	n/a	0.0008	n/a	n/a	n/a	n/a
F4b*	4.4	42	1.4	n/a	0.0009	n/a	n/a	n/a	n/a
	11.4 (RA,	1E							
F5	T1-4)	45 _(RA, T1-4) 46 _(T4v2)	3.8	0.0028	0.0019	0.0020	0.0007	0.0268	0.0273
	22.1 _(T4v2)	. 0(1402)							
F6	2 (RA, T1-4)	45 _(RA, T1-4)	0.7 (RA, T1-	0.0012	0.0006	0.0003	0.0005	0.0113	0.0144
10	1.3 _(T4v2)	41 _(T4v2)	T4v1) 0.6 _(T4v2)	0.0012	0.0000	0.0003	0.0003	0.0113	0.0144
		32 (RA, T1,							
F7	1.9	T2)	0.5	0.0039	0.0113	0.0124	0.0020	0.0077	0.0077
		35 _{(T3, T4,}							
		T4v2) 48 _{(RA, T1,}	4.0 (RA, T1-T2,						
	11.8 (RA,	T3)	T4v1)	0.0000	0.0006	0.0004	0.004.0	0.0040	0.0400
F8	T1-4)	47 _(T2, T4v1)	4.1 _(T3)	0.0032	0.0026	0.0024	0.0010	0.0318	0.0108
	1.7 _(T4v2)	54 _(T4v2)	4.4 _(T4v2)						
		42 (RA, T1,							
F9	10.5	T2)	3.2	0.0017	0.0009	0.0014	0.0003	0.0156	0.0156
		41 _{(T3,} T4v1, T4v2)							
		1401, 1402)							

Table S4.2: Earthquake recurrence intervals for M>4.0, considering the v1 configuration of faults. *F4 rates are the summed values for F4a and F4b for the second time period (192 to 170 Ma).

Fault name	RA: 209.5 to	T1: 209.5 to 192	T2: 192 to 170	T3: 170 to 142.3	T4: 142.3 to
Fault name	137.3 Ma	Ma	Ma	Ma	137.3 Ma

F1 (Single fault)	2,660 yrs	3,410 yrs	3,040 yrs	6,550 yrs	418 yrs
F2	7,030 yrs	22,100 yrs	51,600 yrs	2,920 yrs	1,140 yrs
F3	19,500 yrs	36,800 yrs	47,300 yrs	66,200 yrs	1,820 yrs
F4*	4,060 yrs	73,400 yrs	7,100 yrs	3,330 yrs	639 yrs
F5	4.840 yrs	5,660 yrs	5,370 yrs	15,400 yrs	401 yrs
F6	39,600 yrs	79,100 yrs	15,800 yrs	96,600 yrs	4,200 yrs
F7	11,500 yrs	3,970 yrs	3,620 yrs	24,300 yrs	6,310 yrs
F8	3,350 yrs	4,120 yrs	4,350 yrs	10,300 yrs	328 yrs
F9	7,680 yrs	14,500 yrs	9,330 yrs	42,100 yrs	810 yrs
Cumulative rate	618 years	850 yrs	760 yrs	952 yrs	80 yrs

Figure S4.1: Variation in M>4 recurrence intervals

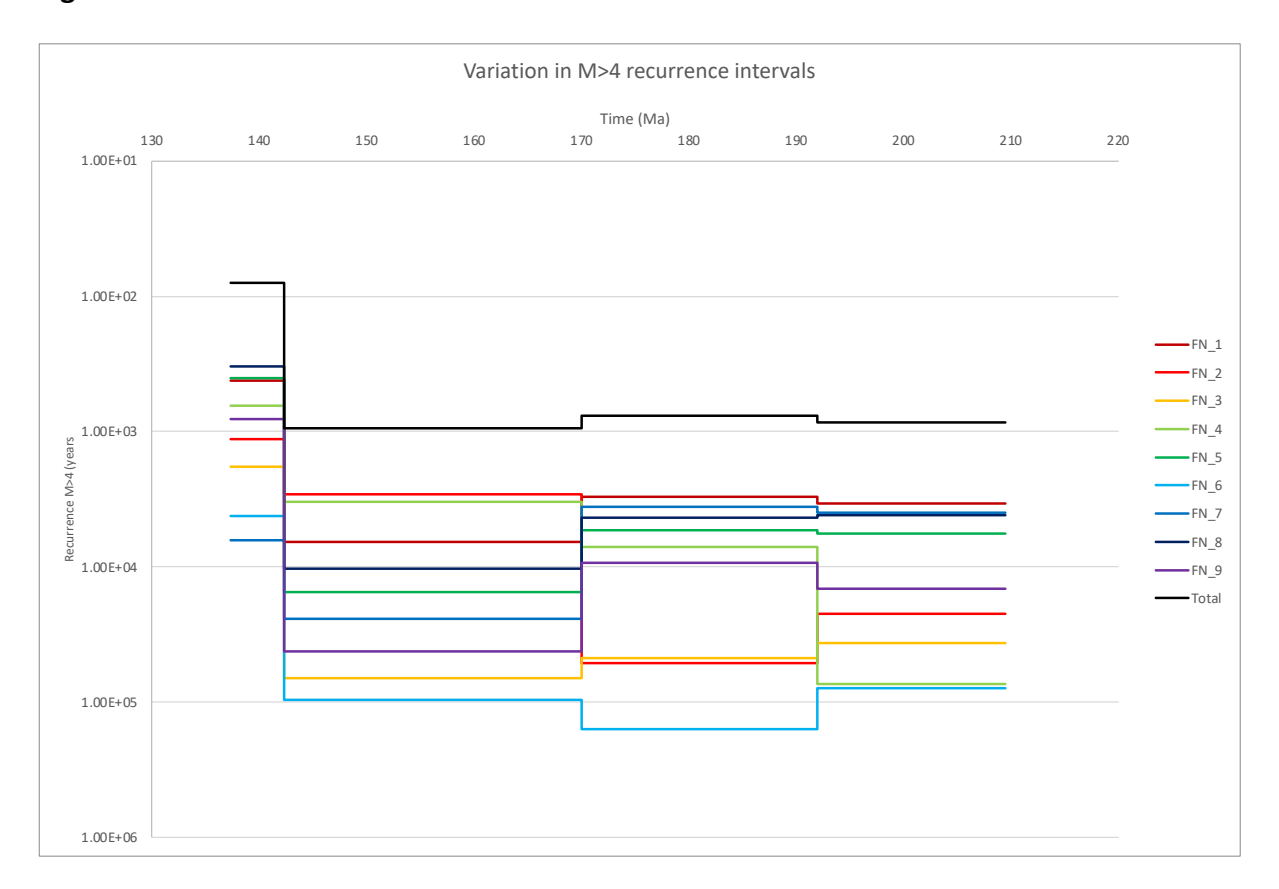


Table S4.3: Earthquake recurrence intervals for M>5.0. *Faults F3, F6 and F7 are too short to generate M>5.0 earthquakes. **F4 rates are the summed values for F4a and F4b for the second time period (192 to 170 Ma).

Fault name*	RA: 209.5 to 137.3 Ma	T1: 209.5 to 192 Ma	T2: 192 to 170 Ma	T3: 170 to 142.3 Ma	T4v1: 142.3 to 137.3 Ma	T4v2: 142.3 to 137.3 Ma
F1 (Single Fault)	27,900 yrs	35,700 yrs	31,900 yrs	68,600 yrs	4,380 yrs	4,520 yrs
F2	91,500 yrs	288,000 yrs	671,000 yrs	38,000 yrs	14,800 yrs	14,800 yrs
F4**	49,700 yrs	690,000 yrs	86,900 yrs	40,400 yrs	7,830 yrs	7,830 yrs
F5	43,400 yrs	63,900 yrs	60,700 yrs	173,000 yrs	4,530 yrs	6,260 yrs
F8	37,800 yrs	46,600 yrs	49,100 yrs	116,000 yrs	3,710 yrs	n/s
F9	86,800 yrs	164,000yrs	105,000 yrs	476,000 yrs	9,150 yrs	9,150 yrs
Cumulative rate	7,820 yrs	13,100 yrs	11,000 yrs	12,200 yrs	977 yrs	1,460 yrs
1.00E+03						
Recurrence M>5 (years)						— FN_1 — FN_2 — FN_4 — FN_5 — FN_8 — FN_8 — Total
1.00E+05						
1 005: 65						

Figure S4.2: Variation in M>5 recurrence rates considering v2 arrangement of faults for the time period 137.3 to 142.3 Ma.

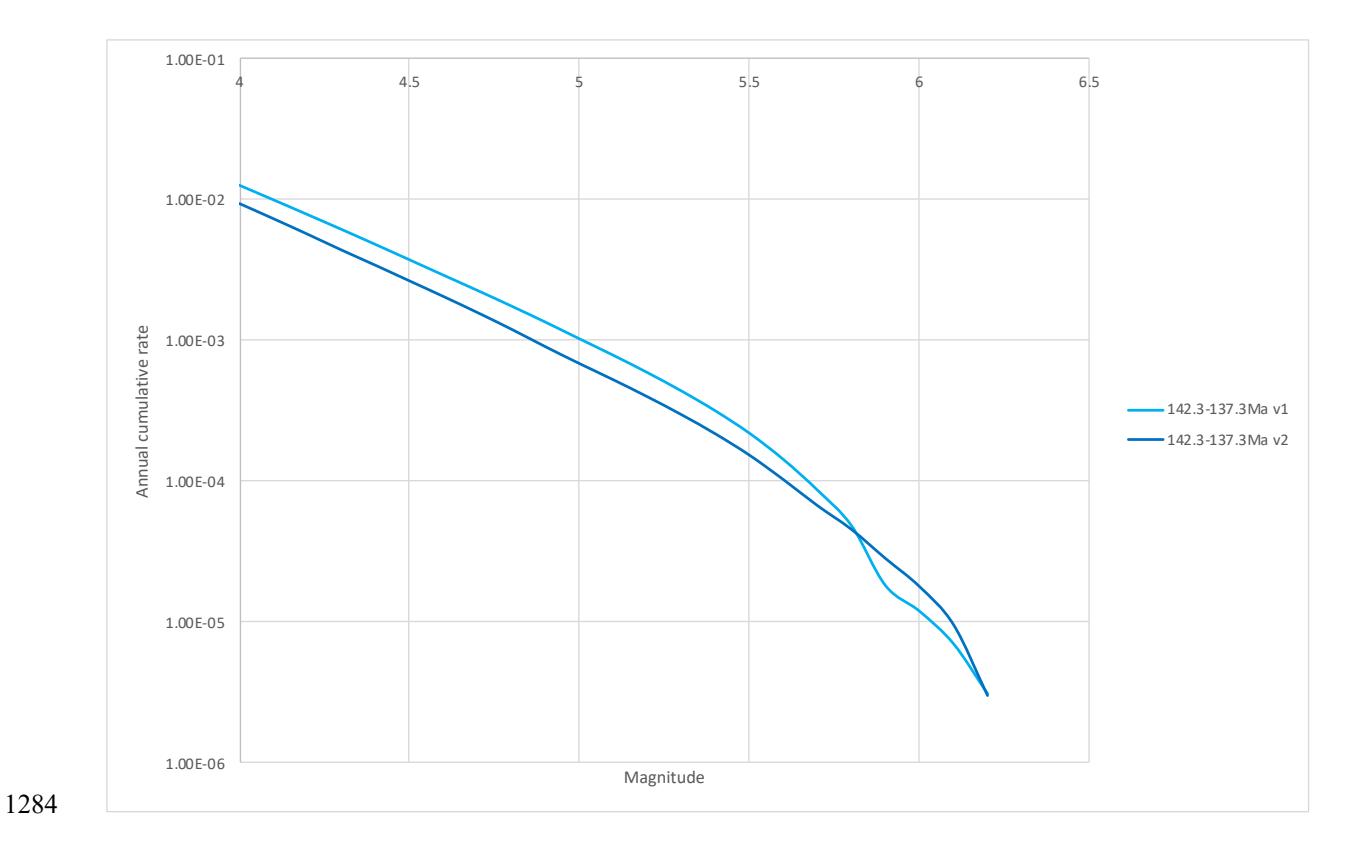


Figure S4.3: Comparison of summed annual cumulative earthquake rates for the 142.3 to 137.3 Ma time period, considering the v1 and v2 arrangement of faults. For all other time periods, see main text, Figure 6b. Note the different inflection points on the graph caused by the changes in fault length and slip rate outlined in Table S4.

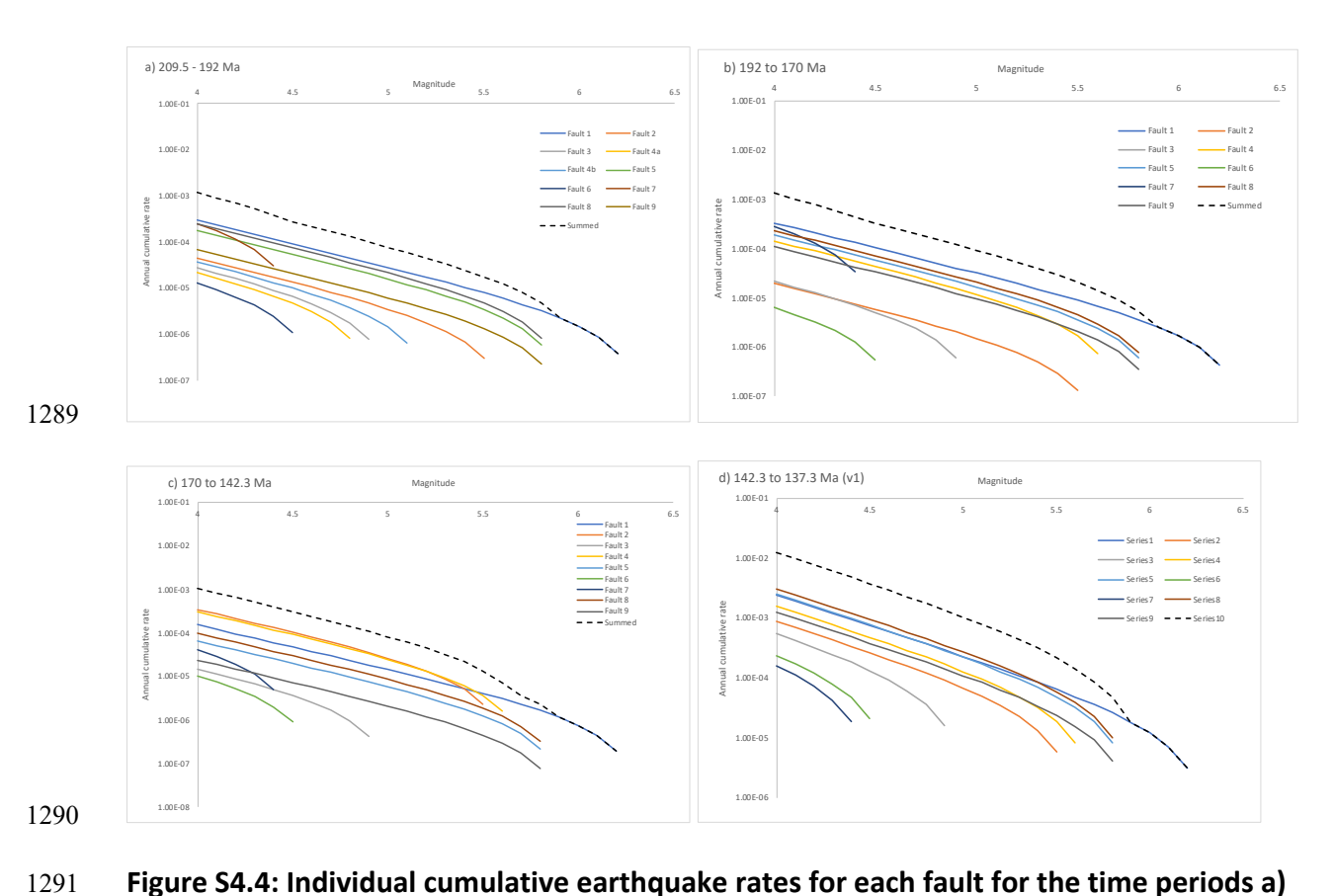


Figure S4.4: Individual cumulative earthquake rates for each fault for the time periods a) 209.5 to 192 Ma; b) 192 to 170 Ma; c) 170 to 142.3 Ma; d) 142.3 to 137.3 Ma.

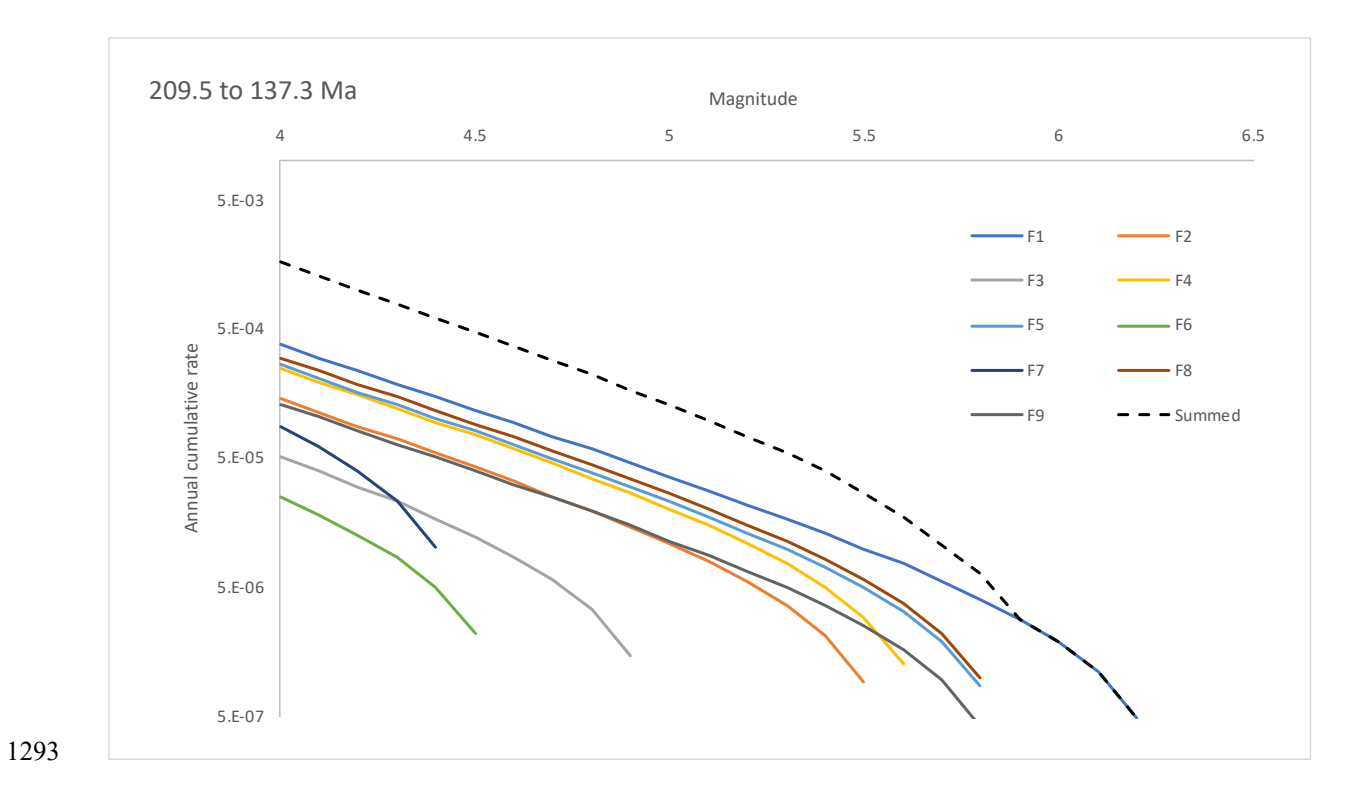


Figure S4.5: Cumulative earthquake rate curves for each fault across the time period 209.5 to 137.3 Ma

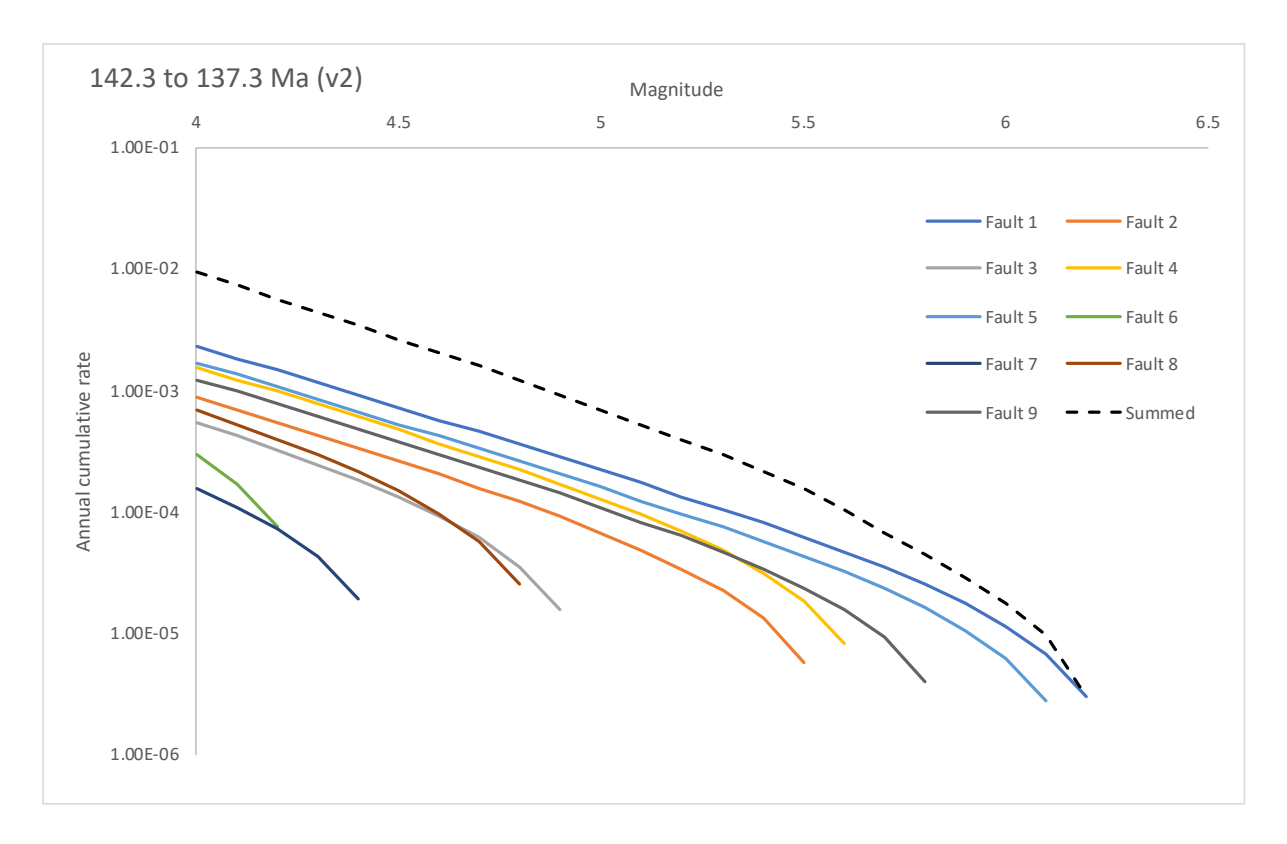


Figure S4.6 Cumulative earthquake rate curves for each fault across the 142.3 to 137.3 Ma time period considering the alternative arrangement of faults.

Supplementary 6: Normalised Slip-rate Variability tables

1299

1300

1301

Table 6.1: Smoothed (n=10) maximum slip-rate by time interval for faults in this study used to calculate normalised slip rate variability (NSRV)

Fault name	Age of the oldest horizon used to calculate slip rate (Myr)	Age of the youngest horizon used to calculate slip rate (Myr)	Length of time window used to calculate slip rate (Myr)	Slip-rate (mm/yr)
Fault 1	209.5	192	17.5	0.00457
Fault 1	192	170	22	0.00440
Fault 1	170	142.3	27.7	0.00206
Fault 1	142.3	137.3	5	0.0407
Fault 1	209.5	137.3	72	0.00524
Fault 1	209.5	142.3	67.2	0.00344
Fault 2	209.5	192	17.5	0.00174
Fault 2	192	170	22	0.000856
Fault 2	170	142.3	27.7	0.00946
Fault 2	142.3	137.3	5	0.0318
Fault 2	209.5	137.3	72	0.00524
Fault 2	209.5	142.3	67.2	0.00527
Fault 3	209.5	192	17.5	0.00166
Fault 3	192	170	22	0.00678
Fault 3	170	142.3	27.7	0.000874
Fault 3	142.3	137.3	5	0.0251
Fault 3	209.5	137.3	72	0.00206
Fault 3	209.5	142.3	67.2	0.000729
Fault 4a	209.5	192	17.5	0.000843
Fault 4b	209.5	192	17.5	0.00139
Fault 4	192	170	22	0.00322
Fault 4	170	142.3	27.7	0.006104
Fault 4	142.3	137.3	5	0.0379
Fault 4	209.5	137.3	72	0.00474
Fault 4	209.5	142.3	67.2	0.00335
Fault 4a_splay	209.5	192	17.5	0.000926
Fault 4_splay	192	170	22	0.00065
Fault 4_splay	170	142.3	27.7	0.00245
Fault 4_splay	142.3	137.3	5	0.00582
Fault 4a_splay	209.5	137.3	72	0.00120
Fault 4a_splay	209.5	142.3	67.2	0.00104

Fault 5	209.5	192	17.5	0.00297
Fault 5	192	170	22	0.0046
Fault 5	170	142.3	27.7	0.00108
Fault 5	142.3	137.3	5	0.0380
Fault 5	209.5	137.3	72	0.00515
Fault 5	209.5	142.3	67.2	0.00458
Fault 5 splay	209.5	192	17.5	0.00136
Fault 5 splay	192	170	22	0.000336
Fault 5 splay	170	142.3	27.7	0.000489
Fault 5 splay	142.3	137.3	5	0.00937
Fault 5 splay	209.5	137.3	72	0.00296
Fault 5 splay	209.5	142.3	67.2	0.000744
Fault 6	209.5	192	17.5	0.00124
Fault 6	192	170	22	0.000298
Fault 6	170	142.3	27.7	0.00117
Fault 6	142.3	137.3	5	0.0175
Fault 6	209.5	137.3	72	0.00119
Fault 6	209.5	142.3	67.2	0.000432
Fault 8	209.5	192	17.5	0.00375
Fault 8	192	170	22	0.00362
Fault 8	170	142.3	27.7	0.00176
Fault 8	142.3	137.3	5	0.0431
Fault 8	209.5	137.3	72	0.00632
Fault 8	209.5	142.3	67.2	0.00445
Fault 8 splay	209.5	192	17.5	0.00105
Fault 8 splay	192	170	22	0.00141
Fault 8 splay	170	142.3	27.7	0.000464
Fault 8 splay	142.3	137.3	5	0.000401
Fault 8 splay	209.5	137.3	72	0.000596
Fault 8 splay	209.5	142.3	67.2	0.000387
Fault 9	209.5	192	17.5	0.00157
Fault 9	192	170	22	0.00176
Fault 9	170	142.3	27.7	0.000524
Fault 9	142.3	137.3	5	0.0220
Fault 9	209.5	137.3	72	0.00256
Fault 9	209.5	142.3	67.2	0.00137
Summed network	209.5	192	17.5	0.00724
Summed network	192	170	22	0.00777

Summed network	170	142.3	27.7	0.0155
Summed network	142.3	137.3	5	0.0816
Summed network	209.5	137.3	72	0.0111
Summed network	209.5	142.3	67.2	0.0132

Table S6.2: Normalised Slip Rate Variability for faults studied in this study across the full time window (i.e., 209.5 to 137.5 Ma).

1302 1303

1304

1305

Fault name	G & D (2021) Slip Rate Variability	Normalised Slip Rate Variability (NSRV)	Fault length (km)	Time averaged slip rate (mm/yr)	Fastest slip rate (mm/yr)	Slowest slip rate (mm/yr)
Fault 1	19.8	7.4	17.7	0.00524	0.0407	0.00206
Fault 2	37.0	5.9	7.4	0.00525	0.0318	0.00086
Fault 3	28.6	11.7	3.3	0.00206	0.0250	0.000874
Fault 4	45.0	7.8	8.3	0.00474	0.0379	0.000843
Fault 4 splay	9.0	4.3	1.6	0.00120	0.00582	0.00065
Fault 5	35.2	7.2	11.4	0.00515	0.0380	0.00108
Fault 5 splay	27.9	3.0	1.2	0.00296	0.00937	0.000336
Fault 6	58.7	14.4	2.0	0.00119	0.0175	0.000298
Fault 8	24.5	6.5	11.8	0.00632	0.0431	0.00176
Fault 8 splay	3.5	1.7	1.9	0.000596	0.00141	0.000401
Fault 9	42.0	8.4	10.5	0.00256	0.0220	0.000524
Summed network	11.3	6.7	25	0.0111	0.0816	0.00724

Table S6.3: Normalised Slip Rate Variability for faults studied across the first three time windows (i.e., 209.5 to 142.3 Ma)

Fault name	G & D (2021) Slip Rate Variability	Slip Rate Variability		Time averaged slip rate (mm/yr)	Fastest slip rate (mm/yr)	Slowest slip rate (mm/yr)	
Fault 1	2.2	0.7	17.7	0.00344	0.00457	0.00206	
Fault 2	11.0	1.6	7.4	0.00527	0.00946	0.000860	
Fault 3	7.8	8.1	3.3	0.000729	0.00678	0.000874	
Fault 4	1.9	0.9	8.3	0.00335	0.006104	0.00322	
Fault 4 splay	3.8	1.7	1.6	0.00104	0.00245	0.000650	
Fault 5	4.3	0.8	11.4	0.00458	0.00460	0.00108	

Fault 5 splay	4.0	1.4	1.2	0.000744	0.00136	0.000336
Fault 6	4.2	2.2	2.0	0.000432	0.00124	0.000298
Fault 8	2.1	0.4	11.8	0.00445	0.00375	0.00176
Fault 8 splay	3.5	2.6	1.9	0.000387	0.00141	0.000401
Fault 9	3.4	0.9	10.5	0.00137	0.00176	0.000524
Summed network	2.1	0.6	25	0.0132	0.0155	0.00724

Table S6.4: Summary statistics by fault type

1306

Fault type	Number of faults	Min NSRV	Max NSRV	Average NSRV
Normal (literature)	116	0.2	8.4	2.0
This study (209.5	11	1.7	14.4	7.1
to 137.3 Ma)				
This study (209.5	11	0.4	8.1	1.9
to 142.3 Ma)				
Strike-slip faults	27	0.2	3.5	1.4
Thrust faults	8	0.3	6.0	2.5

1307 Table S6.5: Literature dataset of slip-rate variability. *N = Normal, S = Strike-slip, T = Thrust.

Fault type*	Location	Fault name	Reference	G & D (2021) Slip Rate Variability	Normalised Slip Rate Variability (NSRV)	Fault length (km)	Time window (Kyr)	Time averaged slip rate (mm/yr)	Fastest slip rate (mm/yr)	Slowest slip rate (mm/yr)
N	My Etna, Italy	Pernicana	D'Amato et al., 2017	7.5	2.6	10	10	2.5	7.5	1.0
N	Kongur Shan Extensional System	Kongur Shan Fault	Ge et al., 2024	10.2	2.4	37	15.2	2.2	5.9	0.58
N	Kongur Shan Extensional System	Eastern Muji Fault	Ge et al., 2024	170.0	2.7	42	16.6	6.3	17.0	0.1
N	Whakatane Graben, NZ	Rangitaiki Fault	Bull et al., 2006	1.7	0.5	20	17.0	3.6	4.6	2.7
N	Taupo Rift, NZ	Paeroa Fault	Nicol et al., 2006	19.5	3.3	30	18.0	0.67	2.34	0.12
N	Taupo Rift, NZ	Ngakuru fault	Nicol et al., 2006	3.2	1.4	18	20	0.22	0.45	0.14
N	Taupo Rift, NZ	Whirinaki Fault	Nicol et al., 2006	5.0	1.5	21	24.0	0.57	1.05	0.21
N	Taupo Rift, NZ	Maleme Fault Zone	Nicol et al., 2006	8.2	3.1	17	25.9	0.42	1.47	0.18
N	Taupo Rift, NZ	W-dipping Maleme Fault Zone	Nicol et al., 2006	4.4	1.4	17	26.0	0.18	0.34	0.078
N	Taupo Rift, NZ	F1	Nicol et al., 2010	n/a	3.2	12	27.0	0.075	0.24	0.0
N	Taupo Rift, NZ	F2	Nicol et al., 2010	n/a	3.1	1	21.4	0.13	0.41	0.0
N	Taupo Rift, NZ	F3	Nicol et al., 2010	n/a	2.1	3	18.0	0.18	0.38	0.0

N	Synthetic	n/a	Nicol et al., 2009	25.5	3.5	10	200	0.14	0.51	0.02
N	Central Apennines, Italy	Assergi	Roberts et al., 2025	3.2	1.8	25	20	0.84	2.22	0.70
N	Central Apennines, Italy	Campo Felice	Roberts et al., 2025	2.7	1.2	11	20	0.57	1.10	0.40
N	Central Apennines, Italy	Colfiorito	Roberts et al., 2025	1.8	0.8	17	20	0.64	1.23	0.69
N	Central Apennines, Italy	Collebrincioni	Roberts et al., 2025	1.8	0.9	37	20	0.44	0.84	0.46
N	Central Apennines, Italy	Frat	Roberts et al., 2025	10.6	2.2	33	20	0.79	1.87	0.18
N	Central Apennines, Italy	Gioia dei Marsi	Roberts et al., 2025	3.3	3.3	41	20	0.95	4.56	1.39
N	Central Apennines, Italy	Larga	Roberts et al., 2025	3.1	1.8	33	20	0.56	1.47	0.48
N	Central Apennines, Italy	Mt d' Ocre	Roberts et al., 2025	3.7	1.7	7	20	0.20	0.46	0.12
N	Central Apennines, Italy	Poggio di Roio	Roberts et al., 2025	3.3	2.0	6.3	20	0.051	0.15	0.045
N	Central Apennines, Italy	Roccacasale	Roberts et al., 2025	5.0	1.7	26	20	0.87	1.82	0.37
N	Central Apennines, Italy	San Sebastiano	Roberts et al., 2025	2.5	1.6	14	20	0.28	0.71	0.28
N	Central Apennines, Italy	Tre Monti	Roberts et al., 2025	3.7	1.3	7	20	0.55	1.03	0.28
N	Taupo Rift, NZ	Maleme Fault, S1	McClymont et al., 2009	8.9	6.1	0.15	24.4	0.17	1.16	0.13
N	Taupo Rift, NZ	Maleme Fault, S2	McClymont et al., 2009	11.7	6.3	0.13	24.4	0.17	1.17	0.1
N	Taupo Rift, NZ	Maleme Fault, S3	McClymont et al., 2009	9.4	4.9	0.25	24.4	0.31	1.69	0.18
N	Taupo Rift, NZ	Rangipo Fault	Villamor et al., 2007	100.0	1.4	32	25	1.4	2.0	0.02
N	Greece	Pisia	Mechernich et al., 2018	5.4	2.8	25	25	0.58	2.0	0.37
N	Gulf of Corinth	DER	Nixon et al., 2024	3.0	1.5	27.8	2000	3.3	7.5	2.5

References

- Bull, J.M., Barnes, P.M., Lamarche, G., Sanderson, D.J., Cowie, P.A., Taylor, S.K. and Dix, J.K.,
- 1310 2006. High-resolution record of displacement accumulation on an active normal fault:
- implications for models of slip accumulation during repeated earthquakes. *Journal of Structural*
- 1312 *Geology, 28*(7), pp.1146-1166

- 1313 D'Amato, D., Pace, B., Di Nicola, L., Stuart, F.M., Visini, F., Azzaro, R., Branca, S. and Barfod,
- D.N., 2017. Holocene slip rate variability along the Pernicana fault system (Mt. Etna, Italy):
- Evidence from offset lava flows. *Bulletin*, 129(3-4), pp.304-317
- Ge, J., Shi, X., Chen, H., Weldon, R., Walker, R., Li, T., Yang, H., Chen, J., Li, F., Wei, X. and Yang,
- 1317 X., 2024. Paleoseismology of the northern Kongur Shan Extensional System, NE Pamir:
- 1318 Implications for potential irregular earthquake recurrence. *Journal of Geophysical Research:*
- 1319 *Solid Earth, 129*(10), p.e2023JB028371
- McClymont, A.F., Villamor, P. and Green, A.G., 2009. Fault displacement accumulation and slip
- rate variability within the Taupo Rift (New Zealand) based on trench and 3-D ground-
- penetrating radar data. *Tectonics*, 28(4)
- Mechernich, S., Schneiderwind, S., Mason, J., Papanikolaou, I.D., Deligiannakis, G., Pallikarakis,
- 1324 A., Binnie, S.A., Dunai, T.J. and Reicherter, K., 2018. The seismic history of the Pisia fault
- 1325 (eastern Corinth rift, Greece) from fault plane weathering features and cosmogenic 36Cl
- dating. Journal of Geophysical Research: Solid Earth, 123(5), pp.4266-4284
- Nicol, A., Walsh, J., Berryman, K. and Villamor, P., 2006. Interdependence of fault displacement
- rates and paleoearthquakes in an active rift. *Geology*, 34(10), pp.865-868
- Nicol, A., Walsh, J., Mouslopoulou, V. and Villamor, P., 2009. Earthquake histories and Holocene
- acceleration of fault displacement rates. *Geology*, 37(10), pp.911-914.
- Nicol, A., Walsh, J.J., Villamor, P., Seebeck, H. and Berryman, K.R., 2010. Normal fault
- interactions, paleoearthquakes and growth in an active rift. Journal of Structural Geology, 32(8),
- 1333 pp.1101-1113
- 1334 Nixon, C.W., McNeill, L.C., Gawthorpe, R.L., Shillington, D.J., Michas, G., Bell, R.E., Moyle, A.,
- Ford, M., Zakharova, N.V., Bull, J.M. and de Gelder, G., 2024. Increasing fault slip rates within
- the Corinth Rift, Greece: A rapidly localising active rift fault network. *Earth and Planetary*
- 1337 *Science Letters, 636*, p.118716
- Roberts, G.P., Iezzi, F., Sgambato, C., Robertson, J., Beck, J., Mildon, Z.K., Papanikolaou, I.,
- 1339 Michetti, A.M., Faure Walker, J.P., Mitchell, S. and Meschis, M., 2025. Characteristics and
- modelling of slip-rate variability and temporal earthquake clustering across a distributed
- network of active normal faults constrained by in situ 36Cl cosmogenic dating of fault scarp
- exhumation, central Italy. *Journal of Structural Geology*, 195, p.105391
- Villamor, P., Van Dissen, R., Alloway, B.V., Palmer, A.S. and Litchfield, N., 2007. The Rangipo
- fault, Taupo rift, New Zealand: An example of temporal slip-rate and single-event displacement

variability in a volcanic environment. *Geological Society of America Bulletin*, 119(5-6), pp.529-